EXPERIMENTAL STUDIES ON SINGLE-MODE AND INTERMODAL NONLINEAR OPTICS IN HIGHER-ORDER-MODE FIBER

A Dissertation

Presented to the Faculty of the Graduate School

of Cornell University

In Partial Fulfillment of the Requirements for the Degree of

Doctor of Philosophy

by

Ji Cheng

May 2012

EXPERIMENTAL STUDIES ON SINGLE-MODE AND INTERMODAL NONLINEAR OPTICS IN HIGHER-ORDER-MODE FIBER

Ji Cheng, Ph. D.

Cornell University 2012

The higher-order-mode (HOM) fiber has recently received great attention due to its special optical properties. The most significant one is its capability of propagating different modes, which is now being utilized to increase data transmission capacity in telecommunication through mode-division multiplexing. Furthermore, the LP_{02} mode of the fiber can be designed to provide dispersion characteristics dramatically different from conventional step-index single-mode fibers (SMFs), such as anomalous dispersion below 1300 nm. This feature has also been widely utilized in a number of applications, including dispersion compensation, high energy pulse-delivery, and nonlinear wavelength conversion. In all the existing applications of the HOM fibers, however, coupling between different guided modes is not desirable, and thus avoided. In order to minimize mode coupling induced by waveguide perturbation, HOM fibers are designed such that the modes have very different effective refractive indices (n_{eff}) at the wavelengths of operation. Consequently, optical effects involve multiple modes, especially multimode nonlinear effects, in the HOM fiber have rarely been explored.

This work focuses on the nonlinear wavelength conversion effects in HOM fibers, including soliton self-frequency shift (SSFS), Cerenkov radiation, and four-

wave mixing (FWM), in both single-mode and multimode schemes. We experimentally demonstrate four nonlinear effects with HOM fibers: 1) SSFS below 800 nm and efficient Cerenkov radiation in the vicinity of 850 nm; 2) high-energy soliton generation at 1080 nm; 3) Intermodal FWM in an all-fiber laser system; 4) Intermodal Cerenkov radiation. In addition, we have developed a convenient dispersion measurement technique specifically tailored for HOM fiber. The results of these experimental demonstrations may lead to potential applications in both biomedical imaging and telecommunication.

BIOGRAPHICAL SKETCH

Ji Cheng was born in Tianmen, Hubei, China on March 28th, 1986 to parents Jiawen Cheng and Xiaoming Lu, who brought him to Beijing a month after. Jiawen, an engineer who is very good with math, and Xiaoming, a chemistry professor who deeply cares about education, started teaching their son arithmetic when he was still a baby. Inevitably, Ji has been okay with math and science but bad with languages, especially English, since his first day at school.

In January 2003, Ji participated in the final competition of China Mathematics Olympics, as one of the 3 players representing the Beijing city. Although the capital did not win the championship in part due to Ji's disappointing performance, Ji still luckily got recruited by Peking University after the competition. In the following summer, Ji graduated from the High School Affiliated to Renmin University, and attended the physics department of Peking University. In the summer of 2005, Ji joined Professor Luhua Lai's research lab, building statistical physics models for protein-folding. Ji's work in biophysics, although was always joked as pseudo-science by his fellow classmates, was his very first research experience.

On April 13th 2007, an unexpected phone call from Ithaca brought Ji to the Cornell Biophysics program, after he almost decided to accept the offer from University of Illinois at Urbana Champaign. During his first year at Cornell, he worked with Professor Michelle Wang and Harold Craighead for rotations. On March 28th 2008, he joined the lab of Professor Chris Xu, where he learned how to burn things with high-power lasers, break optical fibers, or even damage a half-million-dollar laser under the name of fiber optics research. After the wonderful experience in Xu group, Ji plans to move back to Beijing in June 2012 and pursues a different career as a management consultant with the Boston Consulting Group.

ACKNOWLEDGMENTS

The completion of my Ph.D. would not have been possible without the help from my friends and colleagues. I feel really lucky to have the opportunity working with these brilliant minds, and I am extremely grateful for their kind support. First, I would like to thank my advisor Chris Xu, who has given me great guidance in every possible aspect for the last five years. The entire thesis is accomplished under his supervision and based on his ideas and insights in HOM fiber. What's more, he even came into the lab and aligned optics for so many times, just to help on my experiment. His broad knowledge and rigorous working ethics have set us a great example as a scientist. Chris is not only a good teacher, but also a wonderful life mentor. His personal impact on my intelligence, mentality and personality over the last five years is beyond my words. I am certain that the way he thinks, speaks, and works will influence me deeply even after I goes out of school. I want to thank him for his instructions and encouragements, also challenges and tolerance during the time we spent together.

Along the way I've also worked with some great scientists outside of Cornell. I have closely collaborated with researchers from OFS Denmark on all the HOM fiber projects. I am indebted to the scientists at OFS —Martin Pedersen, Lars Grüner-Nielsen, Kim Jesperson, and Dan Jacobsen — for their contribution on these projects. Martin and I share the first-authorship of my last four publications. During the two weeks before the Christmas of 2010, we put in over 200 hours of work while others were enjoying their winter break. However, it is totally worth it. The preliminary results we got during that two weeks eventually became the chapter 3, 4 of this dissertation. Also, Dr. Lars Grüner-Nielsen, who designed the fiber with Martin and supervised these projects with Chris, has also made very significant contribution. It is great honor to work with you two, and I really appreciate your help on this project.

The beginning of graduate school could be hard for lots of people, but for me, with my fellow students in the office, it could not have been any better. I owe the first thanks to Jennifer Lee, who was my student supervisor in my early years, for sharing her patience and kindness, and for sharing her knowledge and expertise. Although Jen has graduated for a while, I still feel sorry for taking so much time away from her own research. I also owe thanks to Demirhan Kobat and David Rivera. I want to thank you guys for everything you did, especially always being positive and cheerful throughout the past years, even during the hardest times. I will also remember and cherish our friendship. I also thank Adam Straub and Dr. Scott Howard for sharing their wisdoms, and answering my stupid questions ranging from optics to English, or even American culture.

In the last two years, fellow student Kriti Charan has joined me in the HOM project. I thank her for all her efforts, including working on experiments with/for me, taking care of all the details and logistics, and especially buying unbelievably cheap equipments on Ebay. I should also thank our postdoc and collaborator Ke Wang, for teaching me optics in Chinese and teasing me with swear words in English. Last but not least, I thank the guys that I have shared office with, Nick Horton, David Huland, Yitang Dai, Zinan Wang, Xianpei Chen, Michael Durst, for all the fun and laughter. It has always been a great time and I will miss you guys for sure.

Finally, I want to thank my friends at Cornell and my family for their support. In all my highs and lows, you have always been there for me. I can never make this far without you. I thank you sincerely.

TABLE OF CONTENTS

LIST OF FIGURES

LIST OF ABBREVIATIONS

CARS	Coherent anti-Stokes Raman scattering
CCD	Charge-coupled device
CFBG	Chirped fiber Bragg grating
CW	Continuous-wave
DMD	Differential mode delay
FWM	Four-wave mixing
FWHM	Full-width at half-maximum
GNLSE	Generalized nonlinear Schrödinger equation
GVD	Group velocity dispersion
HOM	Higher order mode
LPG	Long period grating
MMF	Multimode fiber
OSA	Optical spectrum analyzer
PBGF	Photonic bandgap fiber
PCF	Photonic crystal fiber
SESAM	Semiconductor saturable absorber mirror
SMF	Single-mode fiber
SPM	Self-phase modulation
SRS	Stimulated Raman scattering
SSFS	Soliton self-frequency shift
STED	Stimulated emission depletion
YDFA	Ytterbium-doped fiber amplifier
ZDW	Zero-dispersion wavelength

CHAPTER 1

INTRODUCTION

1.1 Higher-order-mode Fiber

The development of fiber optics is a significant scientific innovation [1], which enables various applications in telecommunications, light generation, sensing, medicine, etc. Many extensively-used technologies, such as wavelength–division multiplexing (WDM), erbium-doped fiber amplifier (EDFA) are developed to facilitate the application of fiber optics, especially in telecommunication.

A conventional optical fiber is a thin strand of glass, which consists of a core with higher refractive index and a surrounding clad with lower index. The core-clad structure functions as an optical waveguide. Similar to the concept of eigenstate in quantum mechanics, light transmitting in the waveguide can propagate with different states, known as modes. The most commonly-used fiber in telecommunication is single-mode fiber (SMF), which only propagates the fundamental eigenstate (i.e., LP_{01} mode). Higher-order-mode fibers, also known as few-mode fibers, are more elaborate fiber devices which can propagate a few modes simultaneously without mode-coupling [2]. The HOM fibers studied in this dissertation support three higher-order-modes (i.e., LP_{02} mode, LP_{11} mode, LP_{21} mode) besides the fundamental mode. These four modes have different spatial power distribution. Thus, in the HOM fiber with appropriately designed refractive index profile, each mode has a different power-weighted average refractive index, which is typically referred as the effective refractive index (n_{eff}). As each mode has its own spatial distribution and n_{eff}, they

possess very different propagation characteristics in the fiber, such as dispersion (i.e. the dependence of light's group velocity on its wavelength) and effective area (i.e. the power-weighted area of the mode).

As HOMs can provide different dispersion from fundamental mode, the LP_{02} mode has been utilized in HOM fibers to achieve anomalous dispersion at wavelengths below 1.3 μm, which is impossible for the fundamental mode in a solid-core step-index SMF [2]. Enabled by this dispersion characteristic, many interesting nonlinear optical phenomena have been demonstrated in HOM fibers, such as soliton self-frequency shift and Cerenkov radiation [3-5].

1.2 Nonlinear optical effects in higher-order-mode fiber

The interaction of light with HOM fibers include linear effects such as dispersion, as well as nonlinear effects such as self-phase modulation, stimulated Raman and Brillouin scattering. These effects, although often considered detrimental to signal transmission in telecommunication, can give rise to many interesting nonlinear optical phenomena, and enable novel light sources based on these phenomena. In this dissertation, we mainly study the nonlinear optical phenomena in HOM fibers arise from the interplay of dispersion, self-phase modulation, and stimulated Raman scattering. The balance between anomalous dispersion and self-phase modulation in an optical fiber allows the generation of an optical soliton, a pulse that maintains its spectral and temporal shape during the propagation [6]. After the formation, the soliton will continuously shift to longer wavelength, due to the stimulated Raman scattering effect [7]. As the soliton red-shifts towards the zero

dispersion wavelength (ZDW), where the fiber transitions from anomalous dispersion to normal dispersion, it generates a phase-matched dispersion wave in the normal dispersion regime, known as the Cerenkov radiation [8]. Besides soliton generation, soliton self-frequency shift, and Cerenkov radiation, we also study two newly-discovered intermodal nonlinear phenomena in a HOM fiber, intermodal Cerenkov radiation and intermodal four-wave mixing (FWM), in this dissertation. These two phenomena are induced by the same nonlinear optical effects. However, the nonlinear phase-matching condition of the two phenomena is fulfilled with multiple modes of the HOM fiber.

This introduction chapter outlines our primary research results on these single-mode or multimode nonlinear phenomena in the HOM fiber. In Chapter 2, I present our effort to generate Cerenkov radiation in HOM fiber at a wavelength of 850 nm. In Chapter 3, we briefly summarize our effort to achieve high-energy soliton using a new HOM fiber design. In Chapter 4, we demonstrated intermodal FWM in an all-fiber system with a HOM fiber. In Chapter 5, a novel optical phenomenon, intermodal Cerenkov radiation, is demonstrated in a HOM fiber. We report our theoretical analysis along with results from experimental measurements. In Chapter 6, we summarize a separate but relevant work to measure the dispersion and modal delay of multiple modes in a HOM fiber using a time-domain technique. Each chapter correlates to a paper that is either published or will be published.

REFERENCES

1. K. C. Kao and G. A. Hockham, "Dielectric-Fibre Surface Waveguides for optical frequencies," *Proceedings of the IEE*, vol. 113, pp. 1151-1158, 1966.

2. S. Ramachandran, S. Ghalmi, J. W. Nicholson, M. F. Yan, P. Wisk, E. Monberg, and F. V. Dimarcello, "Anomalous dispersion in a solid, silica-based fiber," *Opt. Lett.* 31, 2532-2534 (2006).

3. G. P. Agrawal, *Nonlinear fiber optics, 4th* ed. (Academic Press, Boston, 2007).

4. J. van Howe, J. H. Lee, S. Zhou, F. Wise, C. Xu, S. Ramachandran, S. Ghalmi, and M. F. Yan, "Demonstration of soliton self-frequency shift below 1300 nm in higher-order mode, solid silica-based fiber," *Opt. Lett.* 32, 340-342 (2007).

5. J. H. Lee, J. van Howe, C. Xu, and X. Liu, "Soliton Self-Frequency Shift: Experimental Demonstrations and Applications," *J. Sel. Topics in Quantum Elec.* 14-3, 713-723 (2008).

6. J. H. Lee, J. van Howe, C. Xu, S. Ramachandran, S. Ghalmi, and M. F. Yan, "Generation of femtosecond pulses at 1350 nm by Cerenkov radiation in higher-order-mode fiber," *Opt. Lett.* 32, 1053-1055 (2007).

7. J. P. Gordon, "Theory of the soliton self-frequency shift," *Opt. Lett.* 11,662-664 (1986).

8. N. Akhmediev, and M. Karlsson, "Cherenkov radiation emitted by solitons in optical fibers," *Phys. Rev. A* 51, 2602–2607, (1995).

CHAPTER 2

CERENKOV RADIATION AT 850 NM IN HIGHER-ORDER-MODE FIBER

2.1 Introduction

Soliton self-frequency shift (SSFS) and Cerenkov radiation in optical fibers have been theoretically studied [1, 2], and experimentally demonstrated in a variety of fibers in the past [3-10]. It has been shown that a soliton formed in the anomalous dispersion regime can continuously red-shift its central wavelength through the stimulated Raman scattering process. In the case of fibers transitioning to normal dispersion at longer wavelength, SSFS is limited by the second (i.e., at the long wavelength side) zero dispersion wavelength (ZDW). As the frequency-shifted soliton approaches the second ZDW, a phase-matched, red-shifted dispersive wave in the normal dispersion regime, known as Cerenkov radiation, will be emitted by the soliton. The phase-matching condition required for Cerenkov radiation can also be met by the input pulse in the anomalous dispersion regime and a blue-shifted dispersive wave at a wavelength shorter than the first ZDW [9, 11, 12]. As photonic crystal fibers (PCFs) can provide anomalous dispersion in different wavelength regimes, both SSFS and Cerenkov radiation have been previously explored in PCFs at various wavelengths [5, 7, 8, 9, 12]. A number of applications have also been demonstrated using these PCF-based wavelength conversion effects [4, 8, 9].

By propagating light in the LP02 mode, all solid silica-based higher-order-mode (HOM) fibers can be designed to have dispersion characteristics dramatically

different from conventional step-index single-mode fibers (SMFs) [13, 14]. HOM fibers have been engineered to have anomalous dispersion below 1300 nm which was previously possible only with PCFs [15]. This allows HOM fibers to generate SSFS between 1064 nm and 1300 nm [15, 16] and red-shifted Cerenkov radiation generation at 1350 nm [17]. Compared to PCFs, including both index-guided silica-core PCFs and air-core photonic bandgap fibers (PBGFs), HOM fibers are able to generate frequency-shifted solitons and red-shifted Cerenkov radiation at different energy levels [15]. For index-guided silica-core PCFs, the achievable pulse energy of soliton and Cerenkov radiation is restricted by its high nonlinearity, as silica-core PCFs require a small core size to achieve sufficient anomalous dispersion. Approximating these PCF structures by a silica rod surrounded by air, it has been calculated that the maximum core diameter of PCFs is limited to 2.3 μm to obtain anomalous dispersion below 800 nm [18, 19]. This translates to a core size of 4.15 μm^2 and an effective mode area (A_{eff}) of approximately 2 μm^2. To have the second ZDW at 800 nm for the generation of red-shifted Cerenkov radiation at 850 nm, the maximum core diameter is further limited to less than 800 nm, corresponding to an A_{eff} of 0.5 μm^2 [20]. The core size of an actual silica-core PCF exhibiting the same dispersion characteristics would be even smaller. As a result, the pulse energy obtainable in cleanly frequency-shifted solitons in silica-core PCFs is limited to small fractions of a nanojoule [3-8], and the red-shifted Cerenkov radiation in silica–core PCFs demonstrated in previous experiments is below 100 pJ [7, 21]. On the other hand, the pulse energy for solitons in an air-core photonic bandgap fiber (PBGF) is on the order of 100 nJ due to the low nonlinearity of air in the PBGF [22]. The nonlinearity values of HOM fibers lie in-

between silica-core PCF and air-core PBGF as they propagate light in a solid silica core but with a significantly larger A_{eff} than that of silica-core PCFs. Thus, the HOM fiber is able to generate soliton and red-shifted Cerenkov radiation with pulse energy on the order of 1 nJ [16, 17]. Therefore, the HOM fiber is a valuable platform of nonlinear wavelength conversion with pulse energies in-between index-guided silica-core PCFs and air-core PBGFs.

Nonlinear wavelength conversion at or below 850 nm has also been achieved through blue-shifted Cerenkov radiation at a wavelength shorter than the first ZDW [9, 12, 23]. In this case, the required anomalous dispersion regime is shifted to longer wavelengths, reducing the core-size constraints described in the previous paragraph. However, the demonstrated pulse energies in PCFs are still below 100 pJ [9, 12]. Similar blue-shifted Cerenkov radiation with approximately 0.4 nJ pulse energy and 5% conversion efficiency has been generated using highly nonlinear germanosilicate bulk fiber [23]. However, both the pulse energy and the conversion efficiency are significantly lower than red-shifted Cerenkov radiation in HOM fibers. In this paper, we characterize a novel HOM fiber module with a large anomalous dispersion of 120 ps/km/nm and a large A_{eff} of 15 μm^2 at 772 nm (approximately 5 times larger than the A_{eff} of silica-core PCFs designed to have anomalous dispersion below 800 nm). We demonstrate red-shifted Cerenkov radiation generation at 850 nm with 3 nJ pulse energy and up to 60% power conversion efficiency from the input light source (66% photon conversion efficiency) in this module.

2.2 Experimental methods

The experimental setup is shown in Fig. 1(a). An 80 MHz mode-locked Ti:Sapphire laser is used as the input source. The initial pulse launched into the HOM fiber module is centered at 772 nm and has a spectral bandwidth (full width at half maximum, FWHM) of 8 nm. The HOM fiber module consists of a 1.3 m SMF (ClearLite 780-11, OFS), a long period grating (LPG) to convert light from the fundamental mode (LP_{01}) to the LP_{02} mode with more than 99% efficiency between 762 nm and 778 nm, and 5.3 m HOM fiber (FemtoComp 800, OFS). The LP_{02} mode of the HOM fiber has anomalous dispersion between 690 nm and 810 nm [Fig. 1(b)]. The A_{eff} of the LP_{02} mode is between 10 and 15 μm^2 [Fig. 1(c)] in the vicinity of the input wavelength. The input power to the HOM fiber module can be tuned without changing the input polarization by a variable optical attenuator (VOA), which consists of a half-wave-plate and a polarizer. The input pulse is broadened to 300 fs by dispersion in the optical isolator. It is then further broadened to 2 ps by a glass rod to reduce the effects of spectral broadening from self-phase modulation in the SMF pigtail and to protect the LPG from nonlinear photodamage. The output pulse is characterized with an optical spectrum analyzer after collimation. A long pass filter with a cutoff wavelength at 810 nm is used to separate the Cerenkov radiation from the residue input. The pulse energy of the Cerenkov radiation is measured, taking into account the transmission of the long pass filter. The filtered Cerenkov radiation is temporally characterized by a second-order autocorrelator.

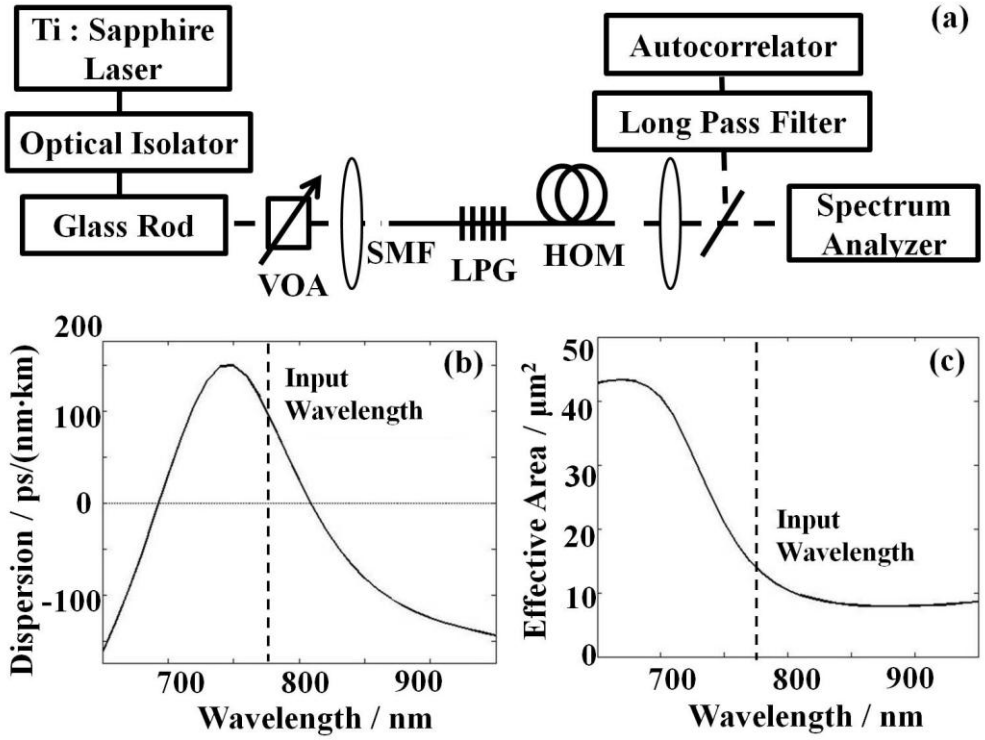

Fig.1. (a) Experimental setup, (b) Calculated dispersion of the LP_{02} mode of the HOM fiber, (c) Calculated A_{eff} of the LP_{02} mode of the HOM fiber.

2.3. Simulated and Experimental results

The fiber propagation process is numerically modeled using the generalized nonlinear Schrödinger equation [24, 25]. The laser source is modeled as a hyperbolic secant pulse with 90 fs FWHM. The pulse is broadened to 2 ps by normal dispersion before entering the HOM fiber module. For propagation in the HOM fiber, our simulation incorporates the contribution of dispersion, self-phase modulation, stimulated Raman scattering, self-steepening, wavelength dependent A_{eff}, and other high order nonlinear effects. The nonlinear refractive index used in the simulation is $n_2=2.0\times10^{-20}$ m^2/W. The dispersion coefficients (up to 14^{th} order) and A_{eff} values are obtained by directly fitting the dispersion and A_{eff} curves shown in Figs. 1(b) and 1(c). The Raman response function is written as

$$R(t) = (1- f_R)\delta(t) + f_R \frac{\tau_1^2 + \tau_2^2}{\tau_1 \tau_2^2} \exp(-\frac{t}{\tau_2}) \sin(\frac{t}{\tau_1}) \Theta(t), \qquad (1)$$

where f_R = 0.18 is the fractional contribution of the delayed Raman response, τ_1 = 12.2 fs, τ_2 = 32 fs, Θ(t) is the Heaviside step function, and δ(t) is the Dirac delta function [25].

We systematically characterize the output spectra at different input pulse energies (from 0.15 nJ to 5 nJ) to show the effects of nonlinear pulse propagation. Spectra measured at 0.2 nm resolution with different input pulse energies are shown in Fig. 2(a). At 0.15 nJ input pulse energy (Fig. 2), a 777 nm frequency-shifted soliton is observed with a pulse energy greater than 0.1 nJ. At higher input pulse energies, the soliton can be further red-shifted, and its wavelength is eventually "locked" at 795 nm at 0.3 nJ input pulse energy (Fig. 2), due to the balance of SSFS and the spectral recoil

from the generation of the Cerenkov radiation. Multiple solitons with spectral overlap are generated at higher input energies. The spectral beating produced by multiple solitons is clearly observable in the spectrum taken at 0.42 nJ input pulse energy (Fig. 2). The measured Cerenkov pulse energy as a function of input pulse energy is shown in Fig. 3. The onset of Cerenkov radiation occurs at approximately 0.22 nJ input pulse energy. A threshold behavior (between input energies of 0.22 nJ and 0.25 nJ) and a plateau behavior (between input energies of 0.25 nJ and 0.4 nJ) are observed at the initial stage of the generation of the Cerenkov radiation, which are consistent with previous observations in PCFs and HOM fibers at other wavelengths [7, 17]. The Cerenkov energy rapidly increases again at 0.4 nJ, indicating the onset of the Cerenkov radiation generated by the second frequency-shifted soliton. These behaviors are all identified in Fig. 3.

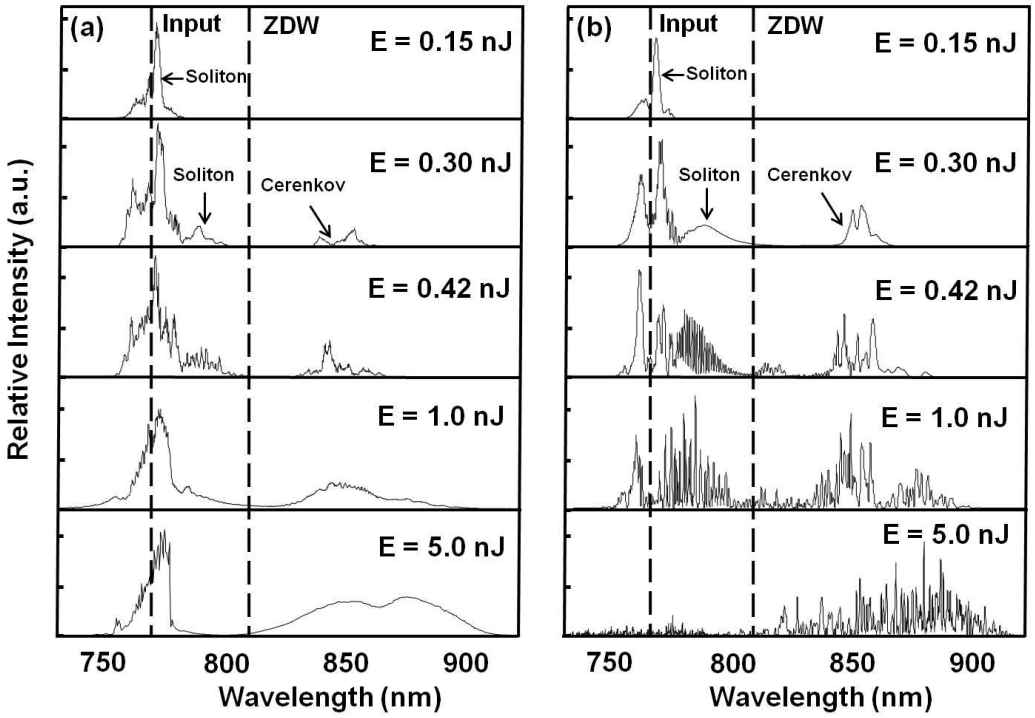

Fig.2. (a) Measured spectra at various pulse energies showing soliton generation, soliton self-frequency shift, and Cerenkov radiation. (b) Simulated spectra with the same input conditions. All traces are taken at 0.2 nm spectral resolution. The soliton and Cerenkov radiation are marked by arrows. The input wavelength and the zero-dispersion wavelength (ZDW) are denoted by dashed lines and the input pulse energy (E) is indicated on each trace.

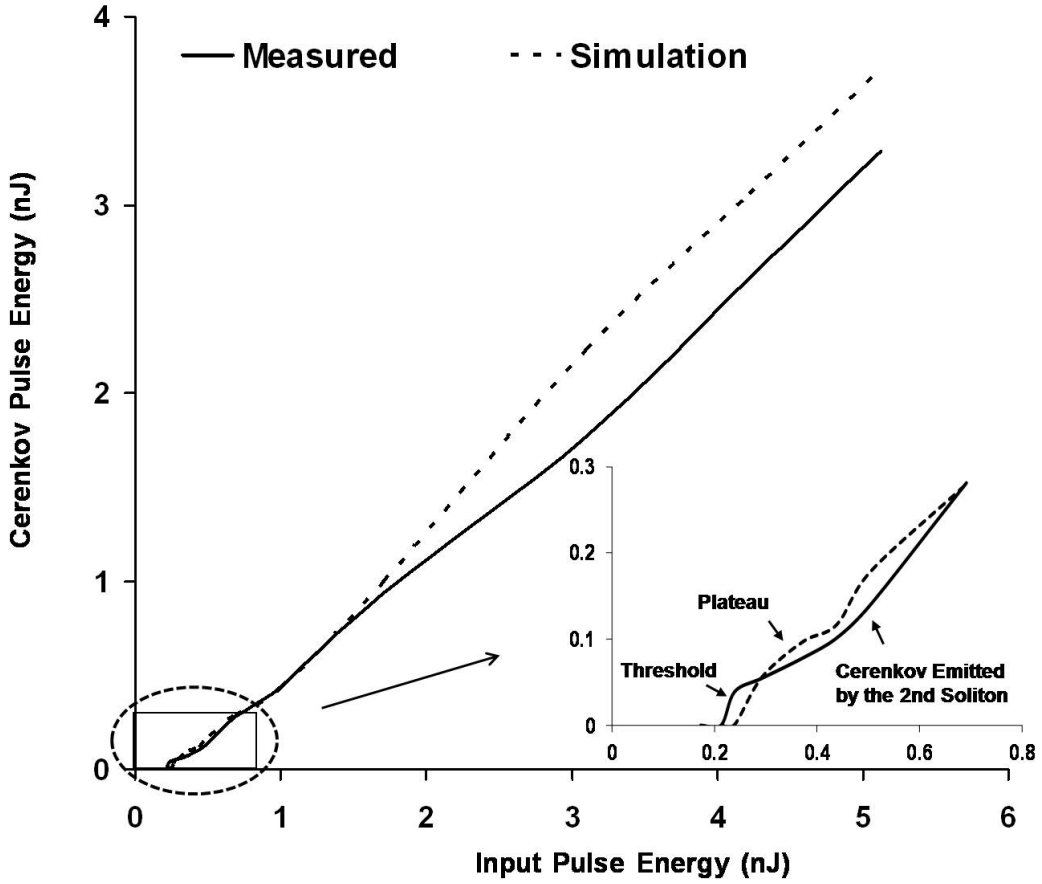

Fig.3. (a) Experimentally measured (solid) and calculated (dashed) Cerenkov pulse energy as a function of input pulse energy. Inset: Experimental results compared with simulated Cerenkov pulse energy at input pulse energies below 0.8 nJ.

To compare with the experimental data, Fig. 2(b) and the dashed line in Fig. 3 show the simulated traces generated using our numerical modeling program. Simulation results are able to match the spectral features and the pulse energies of Cerenkov radiation at input energies from 0.15 nJ to 1 nJ. The simulated spectra at high input energies show many pronounced fine substructures which are extremely sensitive to small changes of the input energy. These fine spectral features were not observed in our experiments. We believe this discrepancy is due in part to the fact that the measured spectra are averaged over many laser pulses at slightly different pulse energies. Similar phenomenon was also theoretically predicted and experimentally observed in previous works on supercontinuum generation [26]. Other discrepancies between the simulated and experimental results are potentially caused by the inaccuracy of the calculated dispersion and A_{eff} curves. Note that at high input energies, simulation also shows 5-10% higher conversion efficiency of the Cerenkov radiation and lower levels of the residue input than the experimental results. This difference might be attributed to the omission of the vectorial nature of the pulse propagation in the HOM fiber in simulation.

At 5 nJ input pulse energy, Cerenkov radiation with 3 nJ pulse energy and 50 nm spectral bandwidth, which translates to a spectral density of 4.8 mW/nm at 80 MHz repetition rate, can be generated without exhibiting super-continuum-like spectral features. The measured and simulated second-order intensity autocorrelation trace of the Cerenkov radiation at 5 nJ input pulse energy is shown in Fig. 4. The measured and simulated traces show FWHM values of 10 ps and 12 ps, respectively. The long pulse duration of the Cerenkov radiation is due to the long propagation

distance (6 m), the broad spectral bandwidth (50 nm), and the high dispersion value of the HOM fiber (100 ps/nm/km). While the Cerenkov energy and its power spectral density can be further increased by using a more energetic input, the potential photo-degradation of the LPGs in the HOM fiber modules prevents us from experimenting at higher input powers.

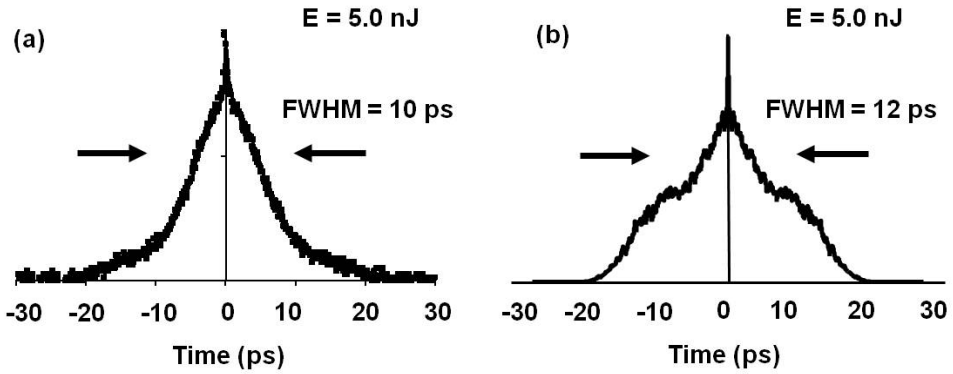

Fig.4. Measured (a) and simulated (b) second-order intensity autocorrelation trace of the Cerenkov radiation at 5 nJ input pulse energy.

2.4. Discussion

Blue-shifted Cerenkov radiation at comparable wavelengths can be generated using the first ZDW of the waveguide. This approach does not require the fiber to achieve anomalous dispersion below 850 nm, and thus the core diameter of the waveguide can exceed 2.3 μm. However, high energy input pulse must be launched at a wavelength much longer than the first ZDW to avoid super-continuum generation, which significantly limits the energy conversion efficiency [9]. More importantly, red-shifted Cerenkov radiation has much higher energy conversion efficiency than blue-shifted Cerenkov radiation because stimulated Raman scattering shifts the pulse towards the longer wavelength and facilitates the energy conversion to the Cerenkov radiation. For example, the results reported by G. Krauss et al. for the blue-shifted Cerenkov radiation at 860 nm have approximately 0.4 nJ pulse energy with an 8 nJ femtosecond input [23]. The red-shifted Cerenkov radiation reported in our paper has approximately 3 nJ pulse energy with a 5 nJ input. Both the conversion efficiency and the absolute pulse energy represent approximately an order of magnitude improvement over the existing results. These improvements are enabled by the unique propagation characteristics of the HOM fiber, which allows us to generate red-shifted Cerenkov radiation in a fiber with a relatively large A_{eff}.

The demonstrated pulse energy and power spectral density of the red-shifted Cerenkov radiation in the HOM fiber is also significantly higher than red-shifted Cerenkov radiation obtainable in PCFs at comparable wavelengths. Because the much smaller A_{eff} of the silica-core PCFs (less than 800 nm core diameter for generating the red-shifted Cerenkov radiation at 850 nm) results in much higher optical nonlinearity,

supercontinuum could be generated by femtosecond input pulses with 1 nJ pulse energy, which results in much lower power spectral density of the Cerenkov radiation. High power spectral density can potentially be achieved in silica-core PCFs with high power continuous-wave input, but the lack of temporal confinement makes the output unsuitable for various applications that require short pulses, such as pump-probe spectroscopy and Coherent Raman Scattering microscopy.

The picosecond Cerenkov radiation generated in the HOM fiber, together with the residue pump light, provides a convenient, synchronized 2-color picosecond source with high pulse energies, which is desirable for a variety of practical applications including pump-probe spectroscopy, modulation transfer microscopy [27], stimulated emission depletion microscopy (STED) [28], etc. The HOM fiber can also be readily integrated with a frequency-doubled femtosecond fiber laser at 775 nm to achieve a fiber-based, picosecond, two-color light source. Although red-shifted CR in an HOM fiber at 1350 nm has been reported in the past, and it is well-known in theory that the wavelength of the CR can be engineered by shifting the dispersion curve, it is challenging to shift the dispersion curve to much shorter wavelengths due to the large increase of the material dispersion. Our results demonstrate that the concept of CR in an HOM fiber can be applied to achieve nonlinear frequency conversion at much shorter wavelengths while maintaining its significant advantages in higher pulse energy and conversion efficiency.

2.5. Conclusion

In summary, we demonstrate SSFS below 800 nm and Cerenkov generation at 850 nm in a solid silica-based HOM fiber module. The HOM module generates significantly more energetic Cerenkov radiation than index-guided silica-core PCFs at comparable wavelengths. We are able to achieve a 3 nJ Cerenkov radiation pulse energy, with high power conversion efficiency of 60% and approximately 4.8 mW/nm spectral density. The HOM fiber module provides a valuable fiber platform for nonlinear wavelength conversion around 800 nm with pulse energies in-between index-guided silica-core photonic crystal fibers and air-core photonic bandgap fibers. This fiber platform can also be tailored to other wavelengths of interest with proper dispersion engineering.

Acknowledgements

This work is supported by grant R21RR024415 from NIH/NCRR. The authors thank Frank Wise and Watt W. Webb for sharing equipment, and John M Dudley for valuable discussions.

REFERENCES

1. J. P. Gordon, "Theory of the soliton self-frequency shift," *Opt. Lett.* 11,662-664 (1986).

2. N. Akhmediev, and M. Karlsson, “Cherenkov radiation emitted by solitons in optical fibers,” *Phys. Rev. A* 51, 2602–2607, (1995).

3. X. Liu, C. Xu, W. H. Knox, J. K. Chandalia, B. J. Eggleton, S. G. Kosinski, and R. S. Windler, “Soliton self-frequency shift in a short tapered air-silica microstructure fiber,” *Opt. Lett*. 26, 358-360 (2001).

4. H. Lim, J. Buckley, A. Chong, and F. W. Wise, “Fiber-based source of femtosecond pulses tunable from 1.0 to 1.3um,” *Electronics Letters* 40, 1523 (2004).

5. N. Nishizawa, Y. Ito, and T. Goto, “0.78-0.90-μm wavelength-tunable femtosecond soliton pulse generation using photonic crystal fiber,” *IEEE Photon. Technol. Lett.* 14, 986-988 (2002).

6. I. Cristiani, R. Tediosi, L. Tartara, and V. Degiorgio, “Dispersive wave generation by solitons in microstructured optical fibers,” *Opt. Express* 12, 124–135 (2004).

7. D. V. Skryabin, F. Luan, J. C. Knight, and P. S. Russell, “Soliton self frequency shift cancellation in photonic crystal fibers,” *Science* 301, 1705–1708, (2003).

8. E. R. Andresen, V. Birkedal, J. Thøgersen, and S. R. Keiding, “Tunable light source for coherent anti-Stokes Raman scattering microspectroscopy based on the soliton self-frequency shift,” *Opt. Lett.* 31, 1328–1330 (2006).

9. H. Tu, and S. A. Boppart, “Optical frequency up-conversion by supercontinuum-free widely-tunable fiber-optic Cherenkov radiation,” *Opt. Express* 17, 9858-9872, (2009).

10. N. Ishii, C. Y. Teisset, S. Kohler, E. E. Serebryannikov, T. Fuji, T. Metzger, F. Krausz, A. Baltuska, and A. M. Zheltikov, "Widely Tunable Soliton Frequency Shifting of Few-Cycle Laser Pulses," *Phys. Rev. E* 74, 036617 (2006).

11. K. Moutzouris, F. Adler, F. Sotier, D. Träutlein, and A. Leitenstorfer, "Multimilliwatt ultrashort pulses continuously tunable in the visible from a compact fiber source," *Opt. Lett.* 31, 1148-1150 (2006).

12. A. V. Mitrofanov, Y. M. Linik, R. Buczynski, D. Pysz, D. Lorenc, I. Bugar, A. A. Ivanov, M. V. Alfimov, A. B. Fedotov, and A. M. Zheltikov, "Highly birefringent silicate glass photonic-crystal fiber with polarization-controlled frequency-shifted output: A promising fiber light source for nonlinear Raman microspectroscopy," *Opt. Express* 14, 10645-10651 (2006)

13. S. Ramachandran, S. Ghalmi, J. W. Nicholson, M. F. Yan, P. Wisk, E. Monberg, and F. V. Dimarcello, "Anomalous dispersion in a solid, silica-based fiber," *Opt. Lett.* 31, 2532-2534 (2006).

14. K. G. Jespersen, T. Le, L. Grüner-Nielsen, D. Jakobsen, M. E. V. Pederesen, M. B. Smedemand, S. R. Keiding, and B. Palsdottir, "A higher-order-mode fiber delivery for Ti:Sapphire femtosecond lasers, " *Opt. Express* 18, 7798–7806 (2010).

15. J. van Howe, J. H. Lee, S. Zhou, F. Wise, C. Xu, S. Ramachandran, S. Ghalmi, and M. F. Yan, "Demonstration of soliton self-frequency shift below 1300 nm in higher-order mode, solid silica-based fiber," *Opt. Lett.* 32, 340-342 (2007).

16. J. H. Lee, J. van Howe, C. Xu, and X. Liu, "Soliton Self-Frequency Shift: Experimental Demonstrations and Applications," *J. Sel. Topics in Quantum Elec.* 14-3, 713-723 (2008).

17. J. H. Lee, J. van Howe, C. Xu, S. Ramachandran, S. Ghalmi, and M. F. Yan, "Generation of femtosecond pulses at 1350 nm by Cerenkov radiation in higher-order-mode fiber," *Opt. Lett.* 32, 1053-1055 (2007).

18. J. C. Knight, J. Arriaga, T. A. Birks, A. Ortigosa-Blach, W. J. Wadsworth, and P. St. J. Russell, “Anomalous dispersion in photonic crystal fiber,” *IEEE Photon. Technol. Lett.* 12, 807- 809 (2000).

19. M.A. Foster and A. L. Gaeta, "Ultra-low threshold supercontinuum generation in sub-wavelength waveguides," *Opt. Express* 12 3137-3143 (2004)

20. M. A. Foster, K. D. Moll, and A. L. Gaeta, "Optimal waveguide dimensions for nonlinear interactions," *Opt. Express* 12 2880-2887 (2004).

21. P. Falk, M. H. Frosz, O. Bang, L. Thrane, P. E. Andersen, A. O. Bjarklev, K. P. Hansen, and J. Broeng, “Broadband light generation around 1300nm through spectrally recoiled solitons and dispersive waves,” *Opt. Lett.* 33, 621–623 (2008).

22. F. Luan, J. C. Knight, P. S. Russell, S. Campbell, D. Xiao, D. T. Reid, B. J. Mangan, D. P. Williams, and P. J. Roberts, “Femtosecond soliton pulse delivery at 800 nm wavelength in hollow-core photonic bandgap fibers,” *Opt. Express* 12, 835–840, (2004).

23. G. Krauss, D. Fehrenbacher, D Brida, C Riek, A Sell, R Huber, and A. Leitenstorfer, “All-passive phase locking of a compact Er:fiber laser system,” *Opt. Lett.* 36, 4, 540-542 (2011).

24. J. Lægsgaard, “Mode profile dispersion in the generalised nonlinear Schrodinger equation,” *Opt. Express* 15, 110–123 (2007).

25. J. M. Dudley, and J. R. Taylor, “Nonlinear fibre optics overview” in *Supercontinuum generation in optical fibers* (Cambridge University Press, 2010), Chapter 3, 33-51.

26. A. L. Gaeta, "Nonlinear propagation and continuum generation in microstructured optical fibers," *Opt. Lett.* 27, 924-926 (2002).

27. C. W. Freudiger, W. Min, B. G. Saar, S. Lu, G. R. Holtom, C. He, J. C. Tsai, J. X. Kang, and X. S. Xie, “Label-free biomedical imaging with high sensitivity by stimulated Raman scattering microscopy,” *Science* 322, 1857-1861 (2008).

28. T. A. Klar, S. Jakobs, M. Dyba, A. Egner, and S. W. Hell, “Fluorescence microscopy with diffraction resolution barrier broken by stimulated emission,” *Proc. Natl. Acad. Sci. U.S.A.* 97(15), 8206–8210 (2000).

CHAPTER 3

HIGH-ENERGY SOLITON GENERATION IN HIGHER-ORDER-MODE FIBER

3.1 Introduction

Soliton self-frequency shift (SFSS), where a femtosecond soliton pulse is excited in a fiber and shifted by intrapulse Raman amplification towards longer wavelengths, are often utilized to make wavelength-tunable femtosecond laser[1,2]. This method naturally requires a fiber with anomalous dispersion to counteract the self-phase modulation for soliton generation. As the zero dispersion wavelength of silica is at1.3 μm and a conventional fiber operated in the fundamental mode will always have normal waveguide dispersion from the waveguide, it is necessary to use more elaborate fibers to achieve net anomalous dispersion below 1.3 μm.

Photonic crystal fibers and higher-order-mode (HOM) fibers can be engineered to achieve anomalous dispersion at wavelength from 0.8 μm to 1.3 μm [2-10]. These fibers have distinctive dispersion and nonlinearity, and can be applied to generate soliton at different energy regimes. The relationship between the parameters of fibers and the solitons are describeed by the soliton condition.

$$P_0 \cdot T_0^2 = \left|\beta_2\right| \Big/ \gamma \propto \left|\beta_2\right| \cdot A_{eff} \qquad (1)$$

Where the peak power and the pulse width of a soliton are given by P_0 and T_0. β_2 is the group velocity dispersion in units of ps^2/m, and γ is the nonlinear fiber parameter, defined as:

$$\gamma = \frac{n_2 w_0}{A_{eff}}$$

where n_2 is the nonlinear refractive effective index, ω_0 is the frequency, A_{eff} is the effective area of the electric field [11].

The energy of the soliton pulse is then given by

$$E_0 = 2 P_0 T_0 \propto \beta_2 / (T_0 \cdot \gamma) \propto \beta_2 A_{eff} / (n_2 T_0) \qquad (2)$$

Consequently, from a fiber design perspective, the significant parameters related to the energy of the soliton are the D, A_{eff}, and n_2 for fibers. A_{eff} of micro-structured PCF is very small, typically on the order of 1 μm^2, and the n_2 of hollow core PCF (i.e. photonic bandgap fiber) is extremely low case, approximately 3 orders of magnitude smaller than that of solid silica. Thus, these two types of PCFs only support soliton with pulse energy at approximately 1 J or 0.1 nJ. In between these two energy regions are the HOM fibers, which has solid silica core and much larger effective area than the micro-structured PCF. In the previous studies, HOM fibers are able to generate soliton with pulse energy of 0.8 nJ at approximately 1064 nm. Compared with the both types of PCFs, the pulse energy provided by the HOM fiber is closer to the desired energy level for biomedical imaging applications (i.e., 5-10 nJ). However, previous studies were not able to generate wavelength-tunable soliton pulse with more than 1 nJ pulse energy. In this work we report upon the result of a new HOM fiber for high energy soliton generation. The HOM fiber is able to achieve larger anomalous dispersion and effective area simultaneously, with the $\beta_2 A_{eff}$ product approximately 6 times as large as the previous HOM fibers. A frequency-shifted soliton with more than 6 nJ pulse energy can be generated in the HOM fiber with a high energy femtosecond laser.

3.2 Theory

According to Eq. (2), the soliton energy can be increased by: (1) increasing the $\beta_2 \cdot A_{eff}$ product; (2) shortening the pulse width T_0. If the pulse width can be infinitely reduced, the attainable soliton energy in HOM fibers can be significantly increased without changing the $\beta_2 \cdot A_{eff}$ product. In a fiber with anomalous dispersion at all wavelengths, a high-energy input pulse can be significantly compressed through the higher-order soliton compression effect, and the temporally-compressed pulse will shift out from the residual spectrum through the soliton fission effect [11].

Assuming an input pulse energy of E_{input} and pulse width of T_{input}, a higher-order soliton is generated in the fiber with GVD β_2 and nonlinearity γ. The soliton order N is defined as $(E_{input} \cdot t_{input} \cdot \gamma/2\beta_2)^{1/2}$. Based on the soliton fission theory, the pulse energy and the pulse width of the first soliton (i.e. the temporally compressed pulse mentioned above), $E_{soliton}$ and $T_{soliton}$, can be calculated as

$$E_{soliton} = E_{input} \cdot (2N - 1)/N^2 \quad (3)$$

$$T_{soliton} = 2\beta_2/(\gamma \cdot E_{soliton}) \quad (4)$$

When N is much larger than 1, Eq. (4) and (5) can be simplified to

$$E_{soliton} \approx 2E_{input}/N \propto E_{input}^{1/2} \quad (3)$$

$$T_{soliton} = N\beta_2/(\gamma \cdot E_{input}) \propto E_{input}^{-1/2} \cdot T_{input}^{1/2} \quad (4)$$

As the input pulse energy increases, the soliton energy and the soliton pulse width should increase and decrease respectively. Thus, in a fiber with anomalous dispersion at all wavelengths, a high-energy soliton can always be generated regardless of its dispersion and nonlinearity by using a sufficiently energetic input source. However, it is not the case in a fiber with limited anomalous dispersion regime. As the input pulse

energy increases, the spectral bandwidth of the soliton and the residual energy also increase. To obtain a clean frequency-shifted soliton, the blue edge of the soliton spectrum needs to be separated from the residual spectrum. On the other hand, the red edge of the soliton spectrum needs to be much shorter than the zero-dispersion wavelength (ZDW) to avoid Cerenkov radiation, which takes energy away from the soliton. As a result, the maximal spectral FWHM soliton is approximately 25 nm for the fiber reported in ref.1, as shown in figure 1, which leads to around 50 fs minimal temporal pulse width.

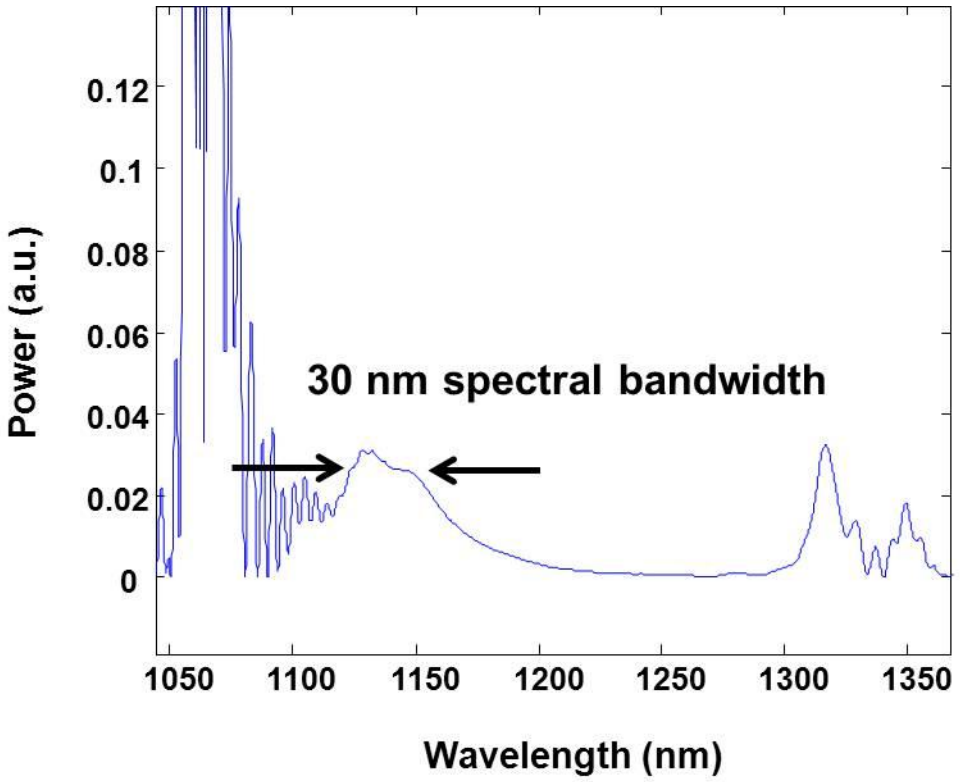

Fig. 1. The available for spectral window for soliton in a HOM fiber with ZDW approximately at 1250 nm.

3.3 Experimental results and conclusion

The temporal pulse width of the soliton cannot be infinitely reduced for high-energy soliton generation, and thus, to increase the soliton energy, it is a matter of designing a fiber, with a very large $\beta_2 A_{eff}$ product for the mode in which the soliton propagates. In this work, we focus on the LP_{02} mode in HOM fiber. In order to enhance the waveguide dispersion of the LP_{02} mode, the fiber has a triple clad design. The parameter space of the design of the HOM fiber has been thoroughly investigated by running numerous computations of different configurations to find the optimum design for the highest soliton energy. The optimized design is a comprise of soliton energy and the wavelength range for SSFS. As we increase the peak value of the β_2, a mode crossing between the LP_{02} mode and LP_{11} mode moves closer to the peak, which is undesirable for a stable operation. Any imperfection in the fabrication process will result in a fiber without perfect cylindrical symmetry, and therefore any mode-crossing could create a strong coupling between the two modes. The mode-crossing limits the wavelength range in which the soliton can be formed and shifted without any significant loss. As a compromise between soliton energy and stability, our optimized design has a mode-crossing between the LP_{02} and LP_{11} modes at around 1120 nm. Fig. 2 shows the effective index as a function of the wavelength for the lowest four propagating LP modes. In this particular design, we are able to achieve anomalous dispersion of 150 ps/(nm km) and an effective area of 100 μm^2 at 1070 nm [12], compared to anomalous dispersion of 50 ps/(nm km) and an effective area of 40 μm^2 in our previous designs. The group velocity dispersion D and effective area of the LP_{02} mode are shown in fig. 3. Fig. 2 and 3 demonstrate that the mode-crossing

wavelength is very close to the wavelength at the peak of the dispersion curve. To best utilize the wavelength regime with high $\beta_2 \cdot A_{eff}$ product, the left hand side of dispersion curve should be used for the soliton shift. In this optimization process we have focused on the LP_{02} mode, however, other HOM can also be utilized. In generaral, the process becomes more complex because more mode-crossing will be involved.

We have fabricated a HOM fiber according to the design shown in Fig. 3. Fig. 4 shows the measured spectrum after 25 cm of the optimized HOM fiber, where the input source is an IMRA FCPA μJewel system at a wavelength of 1045 nm. The FWHM pulse duration of the input pulse is approximately 600 fs and the input pulse energy into the fiber is 23 nJ. Because the fiber is a HOM fiber and the pulse is coupled in from free space, only a fraction of the pulse energy is coupled into the LP_{02} mode. Nonetheless, the LP_{02} mode is the only propagating mode with anomalous dispersion and therefore the only mode that can support a soliton pulse and the subsequent SFSS. Fig. 4 shows the soliton has red-shifted to a center wavelength of 1085nm. The energy of the soliton is measured by recording the total power out of the fiber and the power through a long pass filter with the band edge at 1064nm. This results in a soliton energy of 6.3nJ, which is approximately 6 times higher than the previous record in a solid core fiber at wavelengths below 1300nm. The pulse duration of the soliton pulse is measured by using second order intensity autocorrelation, and the FWHM is 137 fs assuming a $sech^2$ pulse profile (Fig. 4). The second order intensity autocorrelation measurement is done with the long pass filter in place. The small pedestal is mainly due to the spectral broadening of the input pulse by self-phase

modulation, which cannot be filtered out by the long pass filter.

In conclusion, we have optimized the HOM fiber design to achieve an energetic soliton pulse. A new HOM fiber is fabricated according to our design criteria, which enabled an energetic soliton that has an temporal FWHM of 137fs and a record pulse energy of 6.3nJ in a solid core fiber at wavelengths below 1300nm.

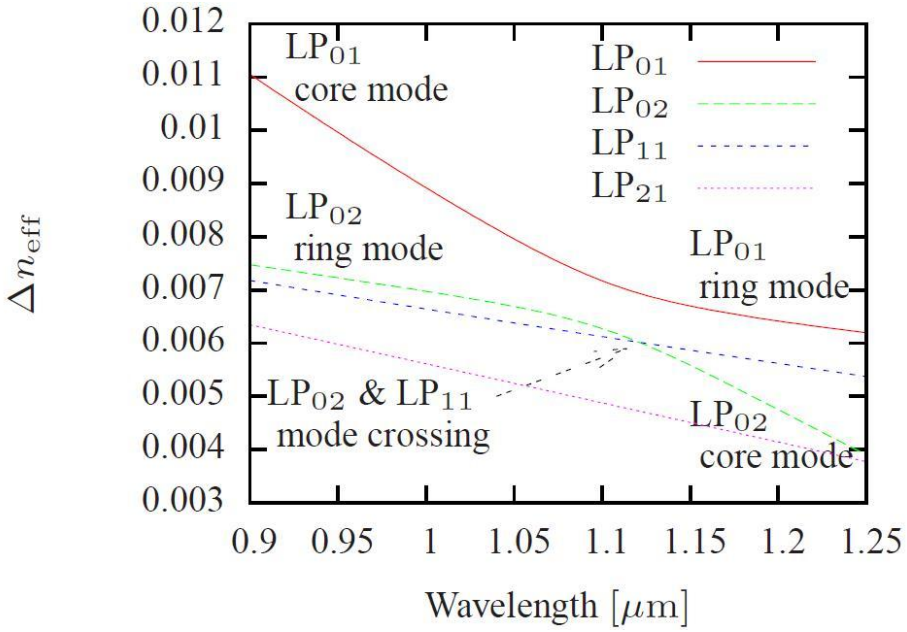

Fig. 2. The effective index for the lowest four propagating modes in the HOM fiber, with respect to pure silica.

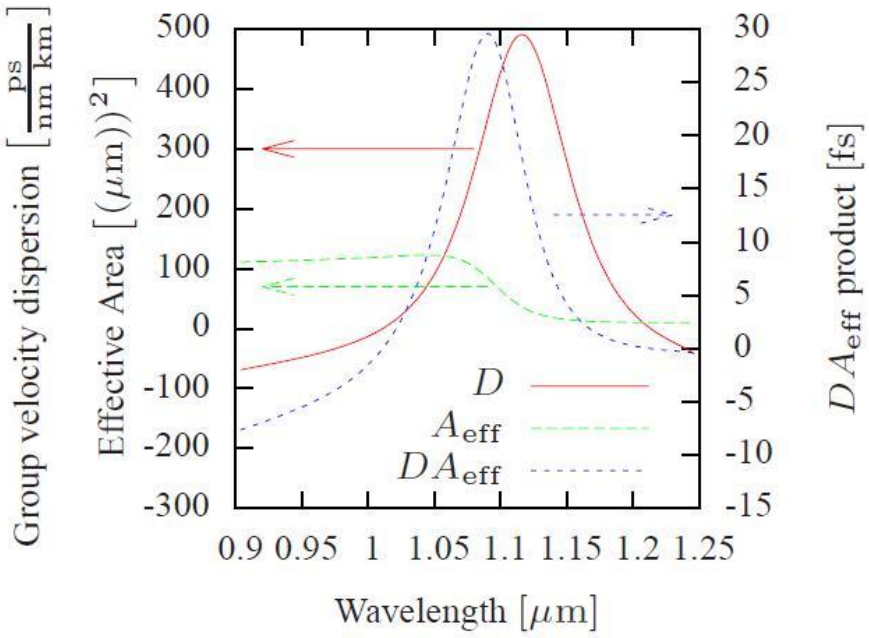

Fig. 3. The dispersion, effective area and DA_{eff} product curves of the LP_{02} mode.

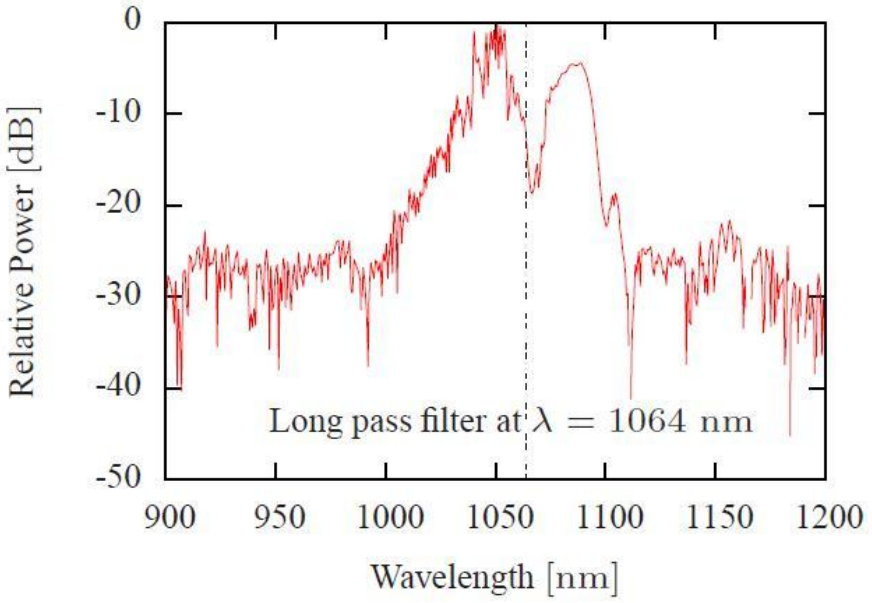

Fig. 4. The measured spectrum with the shifted soliton pulse.

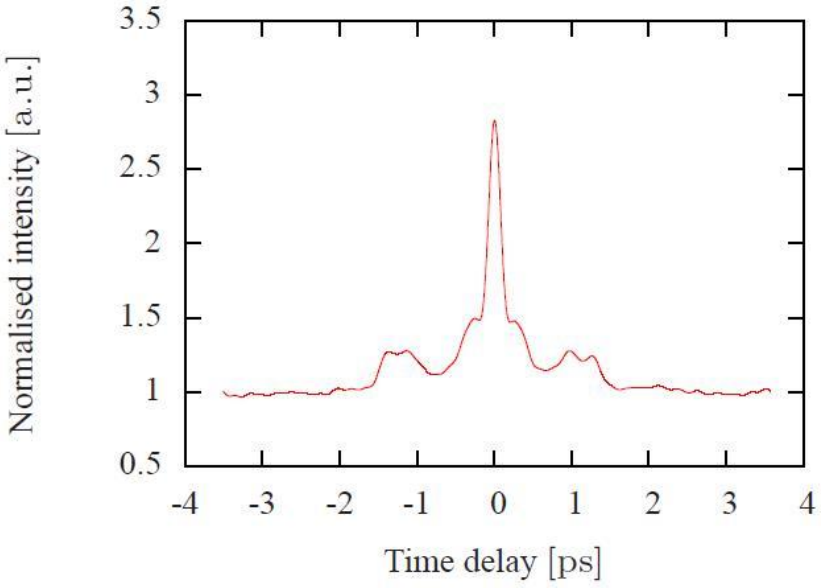

Fig. 5. The measured intensity autocorrelation of the shifted soliton pulse. The measurement is done with the long pass filter in place, but still it can be noticed that there is a small pedestal.

REFERENCES

1. J. P. Gordon, "Theory of the soliton self-frequency shift," *Opt. Lett.* 11,662-664 (1986).
2. J. van Howe, J. H. Lee, S. Zhou, F. Wise, C. Xu, S. Ramachandran, S. Ghalmi, and M. F. Yan, "Demonstration of soliton self-frequency shift below 1300 nm in higher-order mode, solid silica-based fiber," *Opt. Lett.* 32, 340-342 (2007).
3. S. Ramachandran, S. Ghalmi, J. W. Nicholson, M. F. Yan, P. Wisk, E. Monberg, and F. V. Dimarcello, "Anomalous dispersion in a solid, silica-based fiber," Opt. Lett. **31**, 2532-2534 (2006).
4. X. Liu, C. Xu, W. H. Knox, J. K. Chandalia, B. J. Eggleton, S. G. Kosinski, and R. S. Windler, "Soliton self-frequency shift in a short tapered air-silica microstructure fiber," *Opt. Lett.* 26, 358-360 (2001).
5. H. Lim, J. Buckley, A. Chong, and F. W. Wise, "Fiber-based source of femtosecond pulses tunable from 1.0 to 1.3um," *Electronics Letters* 40, 1523 (2004).
6. N. Nishizawa, Y. Ito, and T. Goto, "0.78-0.90-μm wavelength-tunable femtosecond soliton pulse generation using photonic crystal fiber," *IEEE Photon. Technol. Lett.* 14, 986-988 (2002).
7. D. V. Skryabin, F. Luan, J. C. Knight, and P. S. Russell, "Soliton self frequency shift cancellation in photonic crystal fibers," *Science* 301, 1705–1708, (2003).
8. E. R. Andresen, V. Birkedal, J. Thøgersen, and S. R. Keiding, "Tunable light source for coherent anti-Stokes Raman scattering microspectroscopy based on the soliton self-frequency shift," *Opt. Lett.* 31, 1328–1330 (2006).

9. N. Ishii, C. Y. Teisset, S. Kohler, E. E. Serebryannikov, T. Fuji, T. Metzger, F. Krausz, A. Baltuska, and A. M. Zheltikov, "Widely Tunable Soliton Frequency Shifting of Few-Cycle Laser Pulses," *Phys. Rev. E* 74, 036617 (2006).
10. A. V. Mitrofanov, Y. M. Linik, R. Buczynski, D. Pysz, D. Lorenc, I. Bugar, A. A. Ivanov, M. V. Alfimov, A. B. Fedotov, and A. M. Zheltikov, "Highly birefringent silicate glass photonic-crystal fiber with polarization-controlled frequency-shifted output: A promising fiber light source for nonlinear Raman microspectroscopy," *Opt. Express* 14, 10645-10651 (2006)
11. G. P. Agrawal, *Nonlinear fiber optics, 4th* ed. (Academic Press, Boston, 2007).
12. J. Cheng, M. E. V. Perdersen, K. Wang, C. Xu, L. Grüner-Nielsen, and D. Jakobsen, "Time-domain multimode dispersion measurement in a higher-order-mode fiber," Opt. Lett. 37, 347-349 (2012).

CHAPTER 4

INTERMODAL FOUR-WAVE MIXING IN HIGHER-ORDER-MODE FIBER

4.1 Introduction

Four-wave mixing (FWM) in optical fibers has been utilized for nonlinear frequency conversion. FWM has been studied in single-mode fibers, multimode fibers, and more recently, photonic crystal fibers (PCFs) [1-8]. In most experiments, the red-shifted Stokes wave and the blue-shifted anti-Stokes wave are generated within the same mode as the pump light. In these cases, the phase-matching conditions require the pump to be in the vicinity of the zero dispersion wavelength (ZDW) of the propagating mode [8, 9]. However, launching high power pump light near the ZDW can easily generate a supercontinuum (SC), which limits the conversion efficiency from the pump to the narrow-band Stokes and anti-Stokes waves. High-efficiency FWM generation at 673 nm and 2539 nm has been achieved in an endlessly single-mode large-mode-area (LMA) PCF without having the pump light close to the ZDW [10]. However, this approach cannot be extended to generate light at other wavelengths, since the phase-matching condition is predominantly defined by the material dispersion. To overcome the limitation of FWM within a single spatial mode, an intermodal FWM approach has been proposed [11]. In this approach, pump light is launched in the normal dispersion region of the fundamental mode. The Stokes and the anti-Stokes waves can satisfy the phase-matching condition by propagating in other higher-order-modes (HOMs). This effect has been observed in conventional and Ge-doped multimode fibers at visible

wavelengths, using a high power pump at 532 nm [3,4]. Recently, the effect has been studied more systematically in PCFs [11-13].

Intermodal FWM has several advantages over traditional single-mode FWM. This method can achieve high conversion efficiency without SC generation [11]. The wavelength of the Stokes and anti-Stokes light can be easily controlled from tuning the fiber design, such as changing the core diameter [4, 12]. More importantly, this method gives the fiber more degrees of freedom to generate FWM, as the phase-matching condition can be fulfilled with more than one propagating modes. It improves the flexibility for fiber design. However, these experiments require a high-power laser source, such as a Q-switched Nd:YAG laser or a Ti:sapphire regenerative amplifier. As a result, they are typically used to generate light with high pulse energy (~μJ) and low repetition rate (~100 kHz). In addition, the HOMs are only weakly-guided in PCFs, the efficiency of intermodal FWM can be extremely sensitive to perturbations of the fiber. The combination of a high power pump source and PCFs makes the system difficult to be integrated in an all-fiber configuration. In this letter, we demonstrate efficient intermodal FWM in an all-fiber system that consists of a picosecond passive mode-locked fiber laser and a HOM fiber. Compared with previous experiments, intermodal FWM in the HOM fiber requires much lower input pulse energy (~ 20 nJ) and provides much improved stability. The phase-matching condition is fulfilled between two pump photons at 1064 nm in the LP_{01} mode, one anti-Stokes photon in the LP_{01} mode, and one Stokes photon in the LP_{02} mode. The anti-Stokes and Stokes waves are generated, respectively, at 941 nm and 1225 nm with 20% conversion efficiency to each wave. Both waves are in well-guided modes of the HOM fiber, and the large effective refractive index (n_{eff}) difference between modes avoids mode coupling. Due to the characteristics, intermodal FWM in the HOM fiber

has much better stability than in the PCFs. This effect is potentially another valuable application for HOM fibers, which were primarily used for dispersion compensation, soliton generation, and signal transmission [14-16].

4.2 Experimental methods and theoretical calculations

The all-fiber system uses a homemade fiber laser to provide input pulses to the HOM fiber. The fiber laser consists of a SESAM-based laser cavity at 1064 nm, and two ytterbium doped fiber amplifiers (YDFA). The cavity of the oscillator consisted of SMF, Yb-doped gain fiber (Coractive), a SESAM (BATOP) which provided the modelocking mechanism, and a chirped fiber Bragg grating (CFBG, O/E Land). The CFBG reflects 30% of the pulse energy back in the cavity and provides anomalous dispersion for soliton formation. The long fiber length (5.5 m one way) in the cavity not only reduces the repetition rate, but also effectively increases the total nonlinearity, which results in a broader spectral bandwidth. The cavity outputs a 1-nm soliton pulse with an average power of 1 mW at 18.3 MHz repetition rate. Note that further increase the fiber length may cause the cavity difficult to modelock. The first YDFA (pre-amplifier) boosts the oscillator power to 10 mW and the second YDFA (power amplifier) utilized a large-mode-area (10 μm core) double-clad Yb-doped fiber (Liekki) increases the power to 470 mW before the onset of Raman amplification. A single-mode 980 nm fiber-coupled laser diode combined with a fiber wavelength division multiplexer (WDM) coupler is used by the cavity and the first YDFA, and the second YDFA uses a fiber-coupled 976 nm multimode pump diode combined with a high-power signal-pump combiner (ITF Labs). To prevent back-reflection, fiber inline isolators (Novawave) are used between the two amplifiers, and the output of the second YDFA is angle-cleaved. The fiber laser is directly

connected to 1.75 m of HOM fiber, using a core alignment fusion splicer (Fujikura FSM-30S Splicer). After the splice, more than 95% of the power in the HOM fiber is guided in the LP_{01} mode. An optical spectrum analyzer and a second-order autocorrelator are used to characterize the spectral and temporal features of the Stokes and Anti-Stokes pulses. The spatial profiles of the two pulses are magnified by a factor of 100 in a 4F system, and are measured by scanning a 20-μm pinhole with a Germanium photodiode detector. The HOM fiber is designed to have large normal and anomalous dispersion at 1064 nm in the LP_{01} and LP_{02} mode respectively. The calculated neff for the LP_{01} mode and the LP_{02} mode in the HOM fiber is shown in fig. 1(a). The dispersion and group delay derived from the effective refractive indices are in good agreement with experimental measurements[17]. At the pump wavelength of 1064 nm, the LP_{01} mode of the HOM fiber has large normal dispersion, which effectively suppresses SC generation.

To generate a Stokes photon in LP_{02} mode and an Anti-Stokes photon in LP_{01} mode, the propagation constant mismatch $\Delta\beta$, which can be written as $2\beta_{01, P} - \beta_{01,A}(\Omega) - \beta_{02,S}(\Omega)$, must be equal to zero [9]. Here, β is the propagation constant, and the subscripts signify the pump (P), Anti-Stokes (A) and Stokes (S) in the LP_{01} mode (01) and LP_{02} mode (02). Ω is the Stokes shift. $\Delta\beta$ as a function of Ω is derived from the effective refractive index is shown in fig. 1(b). Given the value of β and nonlinearity of the HOM fiber, the nonlinear contribution from the pump light to the phase matching condition can be neglected when the peak power is below 10 kW. When pumped at 1064 nm, the phase-matching condition is satisfied at $\Omega = 2.3\times10^{14}$ rad/s, corresponding to a Stokes wavelength of 1225 nm and an Anti-Stokes wavelength of 941 nm. Note that the anti-Stokes wavelength is highly insensitive to

the pump wavelength, which is similar to the results for intermodal FWM in PCFs [11]. 5 nm shift of the pump wavelength would yield approximately 2-nm shift of the anti-Stokes wavelength and 10-nm shift for the Stokes wavelength.

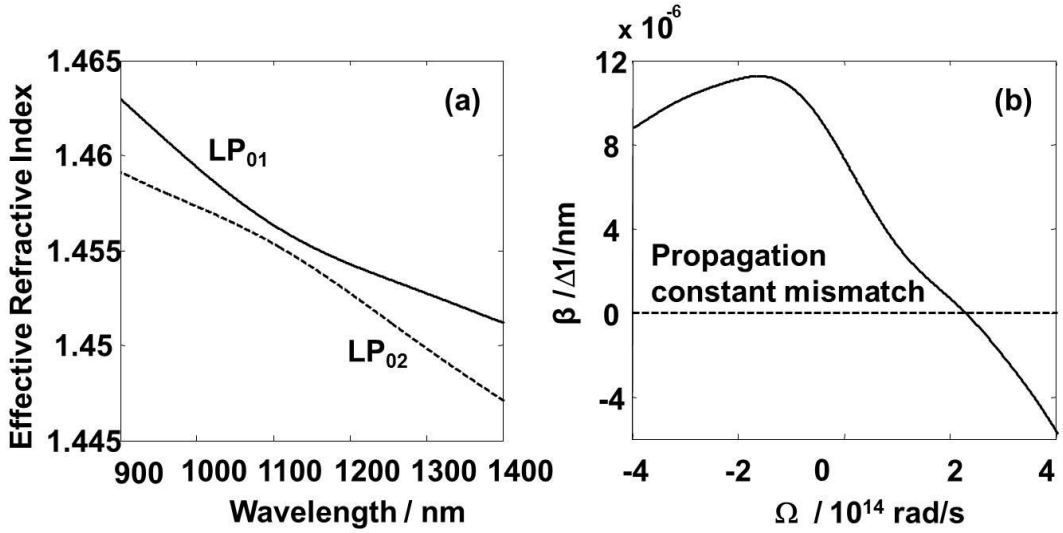

Fig.1(a) Calculated effective refractive indices of the LP_{01}(solid) and LP_{02} (dashed) modes. (b) Propagation constant mismatch, $\Delta\beta$, as a function of Stokes shift Ω, for pump light at 1064 nm.

4.3 Results and discussion

The theoretical prediction of intermodal FWM is validated by our experimental results. Fig. 2 shows the measured spectra at the output of the HOM fiber at various input pulse energies. For pump powers below 200 mW (11 nJ input energy), only SPM-induced spectral broadening can be observed. At 250 mW (14 nJ pulse energy) of pump power, strong, narrowband Anti-Stokes light at 941 nm and broadband Stokes light at 1225 nm are simultaneously generated through FWM. The center wavelengths of both sidebands accurately match our calculation. The bandwidth of the Anti-Stokes light is much narrower than that of the Stokes light since the Anti-Stokes' wavelength is much less sensitive to drift in the pump wavelength than the Stokes' wavelength. This yields a much higher spectral power density in the Anti-Stokes light.

Measured spatial profiles (magnified by 100x) of the anti-Stokes and Stokes light, shown in fig. 3(a) and (b), indicate that they propagate in the LP_{01} and LP_{02} mode, respectively. The measurement results match well with the calculated spatial profiles of the LP_{01} mode at 940 nm and the LP_{02} mode at 1225 nm. The measured profiles show that both waves are tightly confined in the core with a radius smaller than 2 μm. In a HOM fiber, the LP_{02} mode monotonically transitions to the higher-index core from the lower-index ring of the fiber, as the wavelength increases[14]. Consequently, the LP_{02} mode at the Stokes wavelength is very concentrated with approximately 80% of the power in the core, and overlaps significantly with the LP_{01} mode at the anti-Stokes and pump wavelengths. The effective area that represents the spatial overlap of this intermodal FWM process can be written as

$$[\iint_{\infty} F_{01,P}(x,y)\cdot F^{*}_{01,P}(x,y)\cdot F_{01,A}(x,y)\cdot F^{*}_{02,S}(x,y)\cdot dxdy]^{-1}$$

where $F_{01,P}(x, y)$, $F_{01,A}(x, y)$, and $F_{02,S}(x, y)$ are the normalized mode profiles of the pump, anti-Stokes, and Stokes wave, respectively (see derivations from Ref. 3). Based on the spatial distributions of the LP_{01} and LP_{02} mode of the HOM fiber, we obtain a relatively small effective area of approximately 7 μm^2. The small effective area for the intermodal FWM process enables a strong intermodal nonlinear interaction at relatively low input peak power. Hence, spontaneous intermodal FWM can be generated in this HOM fiber at a peak power of just 2 kW, which is 3 orders of magnitude smaller than the peak power required in LMA PCFs at a comparable wavelength. The strong intermodal nonlinearity also ensures a high efficiency for wavelength conversion. With 385 mW (21 nJ pulse energy) coupled into the HOM fiber, approximately 78 mW (4.2 nJ pulse energy) is generated in the anti-Stokes sideband, corresponding to 20% power conversion efficiency. The anti-Stokes pulse has a spectral FWHM of 10 nm, corresponding to 8 mW/nm spectral power density.

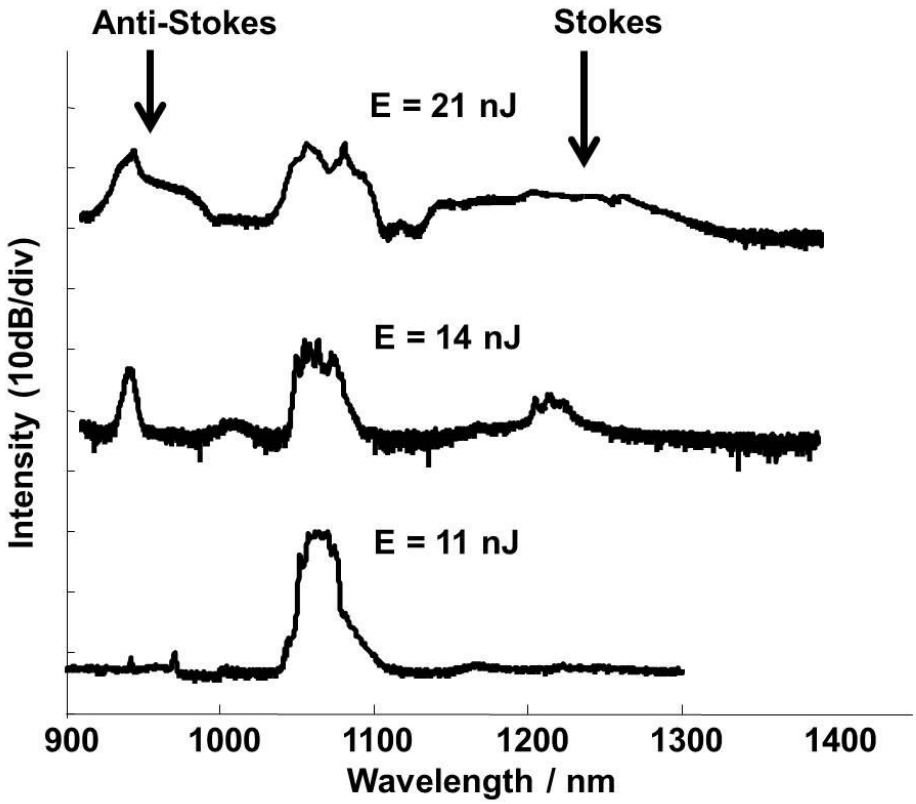

Fig. 2 Output spectra after 1.75 m of HOM fiber with input pulse energies of 11 nJ, 14 nJ, and 21 nJ.

Hence, spontaneous intermodal FWM can be generated in this HOM fiber at a peak power of just 2 kW, which is 3 orders of magnitude smaller than the peak power required in LMA PCFs at a comparable wavelength. The strong intermodal nonlinearity also ensures a high efficiency for wavelength conversion. Up to 385 mW (21 nJ pulse energy) can be coupled into the HOM fiber to achieve this high conversion efficiency. At this input power, approximately 78 mW (4.2 nJ pulse energy) is generated in the Anti-Stokes sideband, corresponding to 20% conversion efficiency. The Anti-Stokes pulse has a spectral bandwidth of 10 nm, corresponding to 8 mW/nm spectral power density.

As the pump in the LP_{01} mode travels at a very different group velocity from the anti-Stokes light in the LP_{01} mode and the Stokes light in the LP_{02} mode, there is significant temporal walk-off between the pump and the anti-Stokes and Stokes pulses generated from the FWM process. Due to the long pulse width of the pump light, the pump can overlap with the FWM waves despite the walk-off, and the efficiency of FWM is not affected. However, the anti-Stokes and Stokes pulses are significantly broadened temporally due to both the temporal walk-off and the group velocity dispersion. The second-order intensity autocorrelation of the anti-Stokes and Stokes light at input pulse energy of 21 nJ are measured and shown in figs.4 (a) and (b), respectively. The FWHMs of the anti-Stokes and Stokes pulses are 16 ps and 13 ps, respectively. The autocorrelation measurement also shows good stability of the anti-Stokes and Stokes pulses. As both the LP_{01} and LP_{02} mode are well-guided in the HOM fibers, the demonstrated intermodal FWM effect is much less sensitive to fiber perturbations than in PCFs, where the anti-Stokes and Stokes bands generated by the intermodal FWM can be significantly attenuated by bending the fiber [11].

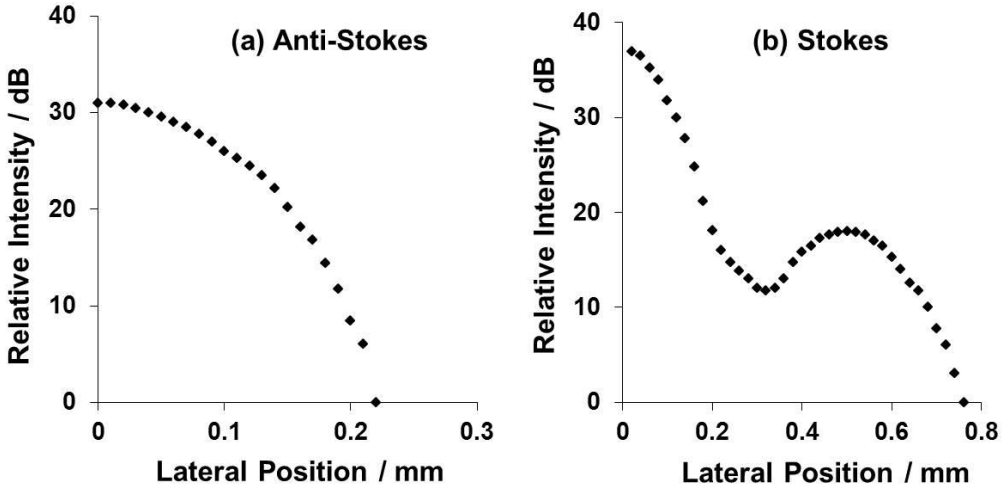

Fig.3 Measured spatial profile of the Anti-Stokes light at 941 nm (a) and the Stokes light at 1225 nm (b), magnified by a factor of 100. Note that the vertical axes are logarithmic.

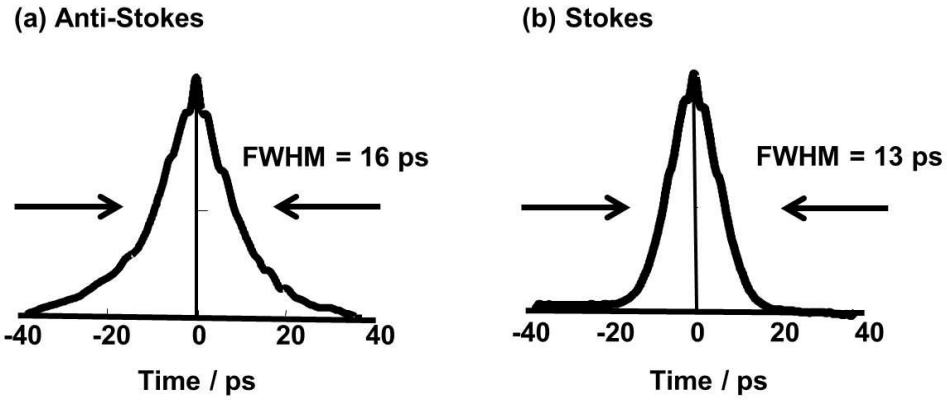

Fig.4 Measured intensity autocorrelation trace of the Anti-Stokes pulse (a) and Stokes pulse (b) at input pulse energy of 21 nJ.

4.4 Conclusion

In conclusion, we demonstrate efficient intermodal FWM in a newly-designed HOM fiber. The all-fiber system based on the HOM fiber can generate Anti-Stokes and Stokes pulses at a distinct regime of pulse energy and repetition rate. Intermodal FWM in the HOM fiber also has better efficiency and stability than the PCFs. This effect provides a new fiber platform for nonlinear wavelength conversion and mode conversion. This fiber platform can be tailored to other wavelengths of interest, such as 1550 nm, with proper dispersion engineering. Its capability to convert signal to a different wavelength and mode efficiently and simultaneously may have applications in existing telecommunication technologies, such as mode division multiplexing and wavelength division multiplexing.

Acknowledgement

The research is supported in part by R01CA133148 and R21RR024415. The authors thank Frank Wise for sharing equipment.

REFERENCES

13. K. O. Hill, D. Johnson, B. S. Kawasaki, and R. I. MacDonald, "CW three-wave mixing in single mode fibers," Journal of Applied Physics, **49**, 5098–5106 (1978).
14. K. Inoue and H. Toha, "Wavelength conversion experiment using fiber four-wave mixing," IEEE Photon. Technol. Lett., **4**, 69-72, (1992).
15. R. H. Stolen, J. E. Bjorkholm, and A. Ashkin, "Phase-matched three-wave mixing in silica fiber optical waveguides," Appl. Phys. Lett. **24**, 308-310 (1974).
16. C. Lin and M. A. Bösch, "Large-Stokes-shift stimulated four-photon mixing in optical fibers," Appl. Phys. Lett. **38**, 479-481 (1981).
17. J. E. Sharping, M. Fiorentino, A. Coker, P. Kumar, and R. S. Windeler, "Four-wave mixing in microstructure fiber," Opt. Lett. **26**, 1048 (2001).
18. J. E. Sharping, Y. Okawachi, J. van Howe, C. Xu, Y. Wang, A. E. Willner and A. L. Gaeta "All-optical, wavelength and bandwidth preserving, pulse delay based on parametric wavelength conversion and dispersion" Opt. Express **13**, 7872-7877 (2005).
19. C. J. McKinstrie, S. Radic and A. R. Chraplyvy, "Parametric amplifiers driven by two pump waves," IEEE J. Sel. Top. Quantum Electron. **8**, 538–547 (2002).
20. W. J. Wadsworth, N. Joly, J. C. Knight, T. A. Birks, F. Biancalana, P. St. J. Russell, "Supercontinuum and four-wave mixing with Q-switched pulses in endlessly single-mode photonic crystal fibers," Opt. Express **12**, 299-309 (2004).
21. G. P. Agrawal, *Nonlinear fiber optics, 4th* ed. (Academic Press, Boston, 2007).
22. D. Nodop, C. Jauregui, D. Schimpf, J. Limpert, and A. Tünnermann, "Efficient high-power generation of visible and mid-infrared light by degenerate four-wave-mixing in a large-mode-area photonic-crystal fiber," Opt. Lett. **34**, 3499–3501 (2009).
23. H. Tu, Z. Jiang, D. L. Marks, and S. A. Boppart, "Intermodal four-wave mixing from femtosecond pulse pumped photonic crystal fiber," Appl. Phys. Lett. **94**, 101109 (2009).

24. A. Labruyere, A. Martin, P. Leproux, V. Couderc, A. Tonello, and N. Traynor, "Controlling intermodal four-wave mixing from the design of microstructured optical fibers," Opt. Express, **16**, 21997–22002 (2008.)
25. C. Lesvigne, V. Couderc, A. Tonello, P. Leproux, A. Barthélémy, S. Lacroix, F. Druon, P. Blandin, M. Hanna, and P. Georges, "Visible supercontinuum generation controlled by intermodal four-wave mixing in microstructured fiber," Opt. Lett. **32**, 2173-2175 (2007)
26. S. Ramachandran, S. Ghalmi, J. W. Nicholson, M. F. Yan, P. Wisk, E. Monberg, and F. V. Dimarcello, "Anomalous dispersion in a solid, silica-based fiber," Opt. Lett. **31**, 2532-2534 (2006).
27. J. van Howe, J. H. Lee, S. Zhou, F. Wise, C. Xu, S. Ramachandran, S. Ghalmi, and M. F. Yan, "Demonstration of soliton self-frequency shift below 1300 nm in higher-order mode, solid silica-based fiber," Opt. Lett. **32**, 340-342 (2007).
28. S. Randel, R. Ryf, A. Sierra, P. J. Winzer, A. H..Gnauck, C. A. Bolle, R.J. Essiambre, D. W. Peckham, A. McCurdy, and R. Lingle, "6×56-Gb/s mode-division multiplexed transmission over 33-km few-mode fiber enabled by 6×6 MIMO equalization", Optics Express **19**, 16697-16707 (2011)
29. J. Cheng, M. E. V. Perdersen, K. Wang, C. Xu, L. Grüner-Nielsen, and D. Jakobsen, "Time-domain multimode dispersion measurement in a higher-order-mode fiber," Opt. Lett. 37, 347-349 (2012).

CHAPTER 5

INTERMODAL CERENKOV RADIATION IN HIGHER-ORDER-MODE FIBER

5.1 Introduction

Light propagation in few-mode fibers, also known as higher-order-mode (HOM) fibers, has recently received great attention due to the possibility of increasing data transmission capacity through mode-division multiplexing[1,2]. However, in order to minimize mode coupling induced by waveguide perturbation, HOM fibers are designed such that the guided modes have very different effective refractive indices (n_{eff}) at the wavelengths of operation[3-5]. Consequently, multimode nonlinear effects and their applications have rarely been explored. In this paper, we demonstrate a novel mode-coupling phenomenon through nonlinear wave mixing in a HOM fiber with a mode-crossing (i.e., two guided modes have the same propagation constant at the same wavelength). A frequency-shifted soliton emits a phase-matched dispersive wave in a different propagating mode. We demonstrate that the mode-crossing in HOM fibers can be utilized to achieve simultaneous wavelength and mode conversion, and the strength of this intermodal nonlinear interaction can be tuned by controlled fiber bending.

5.2 Theory

The nonlinear wave mixing phenomenon reported here is distinct from previous observations in linear propagations (e.g., Ref. 3). Similar to the intermodal four-wave mixing effect[6], the mode coupling is achieved through a nonlinear phase-matching effect involving multiple modes. The phase-matching is realized in the same fashion as dispersive wave generation, also known as Cerenkov radiation, in that an optical soliton perturbed by third- and higher-order dispersion emits a dispersive wave. In a single-mode fiber or within a single mode of a HOM fiber, Cerenkov radiation can be excited at a frequency that is phase-matched with the soliton, when it is near the zero dispersion wavelength[7-13]. However, we show here that the phase-matching condition for intermodal Cerenkov radiation can be satisfied in a HOM fiber when the soliton is in the vicinity of the mode-crossing wavelength, which can be far away from the zero dispersion wavelength. In our HOM fiber, a pump soliton in the LP_{02} mode can generate Cerenkov radiation in the LP_{11} mode. The phases φ of the pump soliton and the Cerenkov radiation at a distance z after a propagation delay $t = z/v_g$ can be written, respectively, as

$$\varphi_{p,02}(\omega_p) = \beta_{p,02}(\omega_p)\cdot z - \omega_p \cdot \frac{z}{v_g(\omega_p)} + \frac{1}{2}\gamma P \cdot z \qquad (1)$$

$$\varphi_{c,11}(\omega_c) = \beta_{c,11}(\omega_c)\cdot z - \omega_c \cdot \frac{z}{v_g(\omega_p)} \qquad (2)$$

where β is the propagation constant and ω is the angular frequency. The subscripts indicate the pump soliton (p) and the Cerenkov radiation (c) in the LP_{02} mode (02) and the LP_{11} mode (11), respectively. $v_g = (d\beta_{p,02}/d\omega)^{-1}$ is the group velocity of the soliton. P and γ are the peak power of the soliton and its nonlinear coefficient, respectively[12]. Given the values of

β and γ in HOM fibers, the nonlinear contribution, which is represented by the last term in equation (1), can be neglected when the peak power is on the order of 10 kW or less, a condition that is well satisfied in our experiments. Based on equations (1) and (2), the phase matching condition $\varphi_c = \varphi_p$ then becomes,

$$\beta_{c,11}(\omega_c) = \beta_{p,02}(\omega_p) + \left.\frac{d\beta_{p,02}}{d\omega}\right|_{\omega_p} \cdot (\omega_c - \omega_p) \qquad (3)$$

The solution of equation (3) can be obtained graphically, as shown in Fig.1a. When the soliton in the LP_{02} mode propagates with anomalous dispersion (i.e., $_{p,02}$ has negative curvature) at ω_p higher than the mode-crossing frequency ω_x, an ω_c lower than ω_x will satisfy equation (3). Thus, a phase-matched, red-shifted intermodal Cerenkov radiation can be generated in the LP_{11} mode by leveraging the presence of the mode-crossing. As in the single mode fiber, the initial photons in the Cerenkov radiation are generated by the nonlinear polarization from the pump photons. Neglecting Raman scattering for simplicity, the evolution of the electric field of the LP_{11} mode can be calculated using the coupled amplitude equation[13].

$$\frac{dA_{c,11}}{dz} = \frac{in_2\omega_c}{c}\left[\left(f_{11}\left|A_{c,11}\right|^2 + 2f_{12}\left|A_{p,02}\right|^2\right)A_{c,11} + 2f_{1112}A_{p,02}A_{p,02}^{*}A_{p,02}e^{i(\varphi_{p.02}-\varphi_{c.11})}\right] \qquad (4)$$

$$f_{1112} = \frac{\left\langle F_{11}^{*}F_{02}^{*}F_{02}F_{02}\right\rangle}{[\left\langle\left|F_{02}\right|^2\right\rangle\left\langle\left|F_{02}\right|^2\right\rangle\left\langle\left|F_{02}\right|^2\right\rangle\left\langle\left|F_{11}\right|^2\right\rangle]^{1/2}}$$

Here $E_j(\vec{r},t) = F_j(x,y)A_j(z,t)e^{i\varphi_j}$ is the electric field, and $F_j(x,y)$ and $A_j(z,t)$ are, respectively, the spatial mode profile and amplitude of electric field of mode j. The phase φ_j *is* defined in equations (1) and (2). The integrals f_{11}, f_{12}, f_{1112} are, respectively, the spatial overlap integrals of self-phase modulation, cross-phase modulation and

four-wave mixing, the last of which is explicitly given in equation (4). The Cerenkov radiation in the LP_{11} mode, $A_{c,11}$, starts at zero, and equation (4) shows that it initially increases at a rate proportional to f_{1112}. Since the LP_{02} and LP_{11} modes have different angular symmetry, their overlap integral, $f_{1112,}$ is zero in a fiber with perfect cylindrical symmetry. Hence, perturbation on the fiber and the mode profile is necessary to make f_{1112} non-zero. As demonstrated in both SMFs and multimode fibers, bending can deform the spatial profiles of guide modes and shift them away from the axis of the fiber[14-16]. The deformation creates a nonzero spatial overlap between the LP_{02} and LP_{11} modes, and can be utilized along with the mode-crossing to control the generation of intermodal Cerenkov radiation in a HOM fiber.

5.3 Experimental Methods

The experimental setup for intermodal Cerenkov radiation is shown in Fig.1b. The HOM fiber under test is designed to generate high energy frequency-shifted soliton[16] . Figs. 1c and 1d present, respectively, the calculated n_{eff} and dispersion curves of the LP_{02} and LP_{11} modes. These dispersion values have been verified by experimental measurements[16]. Between 1000 and 1200 nm, the LP_{02} and LP_{11} modes have anomalous and normal dispersion, respectively. With an input pulse energy of 14.4 nJ and propagation distance of 90 cm, a 4-nJ soliton in the LP_{02} mode is generated at approximately 1085 nm. Through intrapulse Raman scattering, the soliton will red-shift towards the mode-crossing wavelength between LP_{02} and LP_{11} at 1120 nm.

The excitation source for the intermodal Cerenkov generation is an IMRA FCPA μJewel D400 laser, which outputs in free space a 1-MHz pulse train at 1045 nm. The pulses have an autocorrelation FWHM of 600 fs. The power coupled into the fiber is controlled by a variable optical attenuator, which consists of a half-wave-plate and a linear polarizer. An achromatic objective (DIN 4, Edmund Optics) couples light into 90 cm of the HOM fiber mounted on a three-axis NanoMax stage (Thorlabs). The position of the fiber end is optimized to achieve maximal excitation in the LP_{02} mode. The output of the HOM fiber is characterized by an optical spectrum analyzer with 0.5 nm resolution and a second-order autocorrelator. The spatial profile of the fiber output is magnified by a factor of 250 in a 4f imaging system, and recorded by a CMOS CCD camera (DCC1545M, Thorlabs).

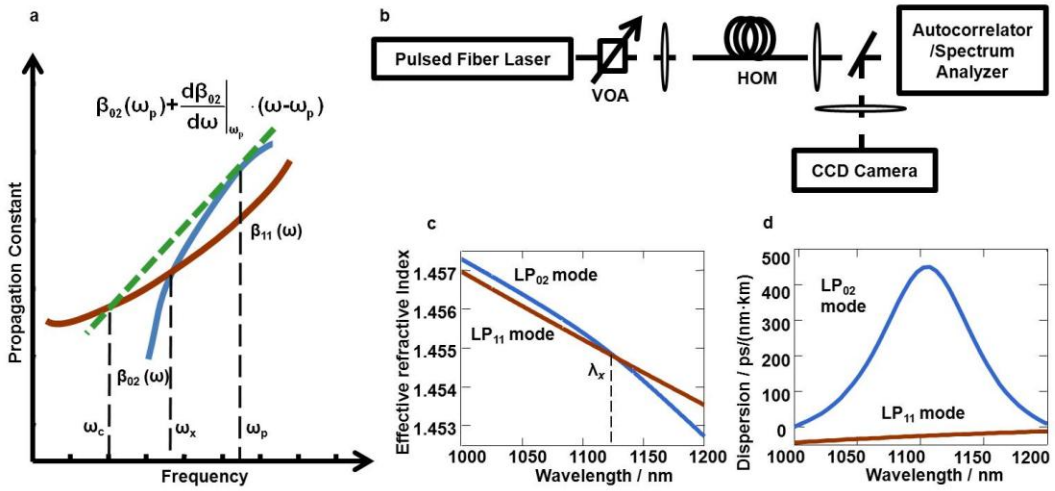

Figure 1. Theory and experimental configuration for intermodal Cerenkov radiation in the HOM fiber. a, Phase-matching condition between Cerenkov radiation in the LP_{11} mode at ω_c and the pump soliton in the LP_{02} mode at ω_p, from equation (3). Schematic drawing of the curves for the propagation constants of the LP_{02} and LP_{11} modes are shown in the vicinity of the mode-crossing frequency ω_x. **b**, Experimental setup for intermodal Cerenkov radiation in the HOM fiber. VOA, variable optical attenuator. **c**, The effective refractive index of the LP_{02} and LP_{11} mode of the HOM fiber in our experiment. λ_x, mode-crossing wavelength. **d**, Dispersion curves of the HOM fiber.

The output spectra are measured with the fiber coiled with different radii to generate intermodal Cerenkov radiation. In a straight HOM fiber, the central wavelength of the soliton can be continuously tuned between 1085 nm and 1120 nm (Fig.2a). Note that mode coupling induced by microbending of the fiber produces spectral modulation on the soliton at the mode-crossing wavelength of 1120 nm. However, Cerenkov radiation in the LP_{11} mode cannot be observed and the output remained in the LP_{02} mode in the straight fiber at all launch powers tested. This observation is consistent with the theoretical prediction that the modal overlap integral vanishes without significant perturbation when using a straight fiber. By bending the HOM fiber, however, the mode overlap integral no longer vanishes, resulting in intermodal nonlinearity for efficient generation of Cerenkov radiation. Figs. 2b and 2c show the experimental results at two bending radii. At 18 nJ input pulse energy and a bending radius of 14 cm, Cerenkov radiation in the LP_{11} mode can be observed at wavelengths beyond 1130 nm. The Cerenkov radiation becomes more pronounced when the bending radius is reduced to 5.5 cm (Fig. 2c). The wavelength separation between the Cerenkov radiation and the soliton increases when decreasing the bending radius, which is consistent with spectral recoil. Higher intermodal nonlinearity caused by the strong perturbation of a sharply-bent fiber can produce more energetic Cerenkov radiation and a stronger spectral recoil effect[11]. The soliton will be frequency-locked at a shorter wavelength by the Cerenkov radiation which in turn will lock at a longer wavelength. In addition, dispersion and n_{eff} change induced by bending can affect the spectral features of the Cerenkov radiation. Our experiments show that the strength of intermodal nonlinear interaction can be effectively tuned by

controlling the bending of the fiber. We experimentally verified that different input polarizations do not affect the spectral evolution and the wavelength of Cerenkov radiation, indicating that the intermodal Cerenkov radiation created by waveguide bending is not a polarization effect. We quantitatively characterize the Cerenkov radiation in the HOM fiber with 5.5 cm bending radius. At 21 nJ input energy, a 6 nJ soliton at 1093 nm excites a 1.5 nJ Cerenkov pulse in the LP_{11} mode at 1140 nm. The measured wavelength of the Cerenkov radiation is in excellent agreement with the theory, which predicts a phase-matching wavelength of 1142 nm based on Equation (3) and the calculated n_{eff}. The measured optical spectrum and the spatial profiles of the soliton and the Cerenkov radiation are presented in Fig. 3(a). We performed second-order intensity autocorrelation measurement, and determined that the pulse width of the Cerenkov radiation is 5.8 ps, as shown in Fig. 3(b). The Cerenkov pulse broadens due to dispersion in the LP_{11} mode and to the temporal walk-off between the soliton and the Cerenkov radiation.

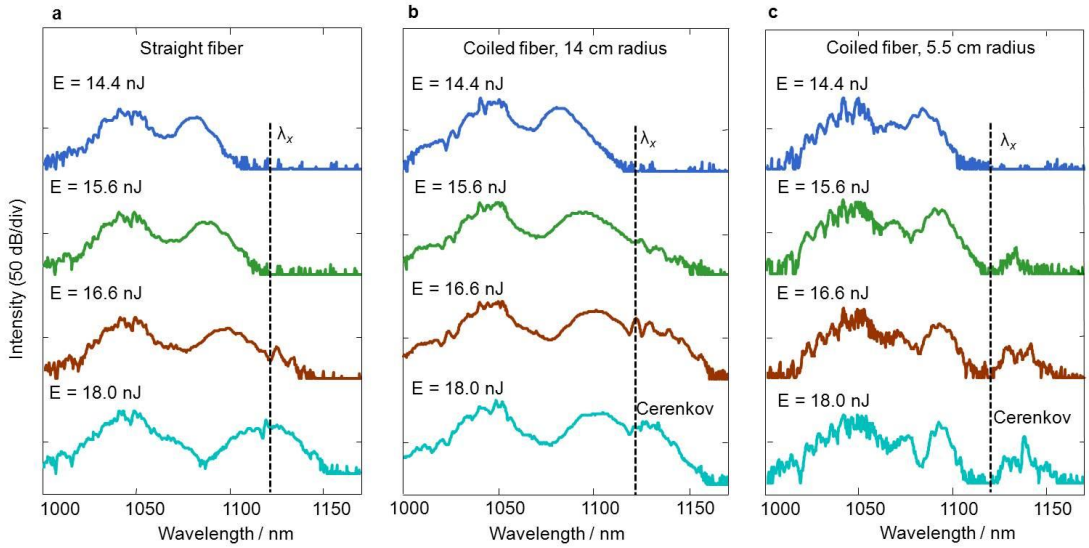

Figure 2. Intermodal Cerenkov radiation in the HOM fiber with different bending radii. **a,** Measured spectra for soliton shift and Cerenkov radiation at different pulse energies in a straight fiber, **b**, fiber coiled with a radius of 14 cm and **c**, 5.5 cm. Cerenkov radiation is labeled at 18.0 nJ input energy. Note that the vertical axes are in logarithmic scale.

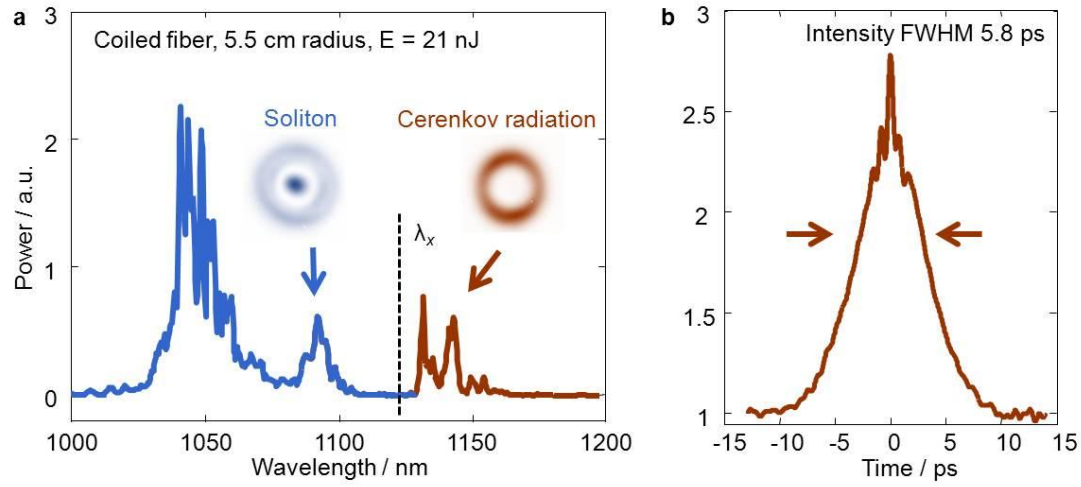

Figure 3. Measured spatial, spectral, temporal profile of the Cerenkov radiation. a, Measured output spectrum of the HOM fiber at 21 nJ input pulse energy. Insets: measured spatial profiles of the soliton and Cerenkov radiation. **b**, Measured intensity autocorrelation trace of the Cerenkov radiation.

5.4 Conclusion

We demonstrate intermodal Cerenkov radiation in a HOM fiber for the first time to the best of our knowledge. The phase-matching condition of such an intermodal nonlinear interaction can be satisfied in the vicinity of the mode-crossing wavelength of the HOM fiber. We show that the intermodal nonlinearity for energy conversion can be created and controlled by tuning the bending radius of the fiber. This novel nonlinear phenomenon can be easily extended to the telecommunication wavelengths by fabricating new HOM fibers. The demonstrated capability of simultaneous mode and wavelength conversion of the HOM fibers may have potential impact in future telecommunication systems based on both mode division multiplexing and wavelength division multiplexing.

Acknowledgements

The research is supported in part by NIH R01CA133148 and R21RR024415. The authors thank Chris Schaffer for sharing equipment.

REFERENCES

[1] C. Koebele *et al*. "Two mode transmission at 2x100Gb/s, over 40km-long prototype few-mode fiber, using LCOS-based programmable mode multiplexer and demultiplexer." *Opt. Express* **19,** 16593-16600 (2011).

[2] S. Randel *et al*. "6×56-Gb/s mode-division multiplexed transmission over 33-km few-mode fiber enabled by 6×6 MIMO equalization." *Opt. Express* **19,** 16697-16707 (2011).

[3] R. Olshansky. "Mode coupling effects in graded-index optical fibers." *Appl Opt.* **14,** 935-945 (1975).

[4] F. Yaman. *et al*. "10×112 Gb/s PDM-QPSK transmission over 5032 km in few-mode fibers." *Opt. Express* **18,** 21342-21349 (2010).

[5] S. Ramachandran. *et al*. "Anomalous dispersion in a solid, silica-based fiber." *Opt. Lett.* **31,** 2532-2534 (2006).

[6] N. Akhmediev, & M. Karlsson. "Cherenkov radiation emitted by solitons in optical fibers." *Phys. Rev. A*, **51,** 2602–2607, (1995).

[7] J. van Howe *et al*. "Demonstration of soliton self-frequency shift below 1300 nm in higher-order mode, solid silica-based fiber." *Opt. Lett.* **32**, 340-342 (2007).

[8] J. H. Lee *et al.* "Generation of femtosecond pulses at 1350 nm by Cerenkov radiation in higher-order-mode fiber." *Opt. Lett.* **32**, 1053-1055 (2007).

[9] J. Cheng *et al. "*Generation of Cerenkov radiation at 850 nm in higher-order-mode fiber." *Opt. Express* **19,** 8874-8880 (2011).

[10] I. Cristiani., R. Tediosi, L. Tartara & V. Degiorgio. "Dispersive wave generation by solitons in microstructured optical fibers." *Opt. Express* **12**, 124–135 (2004).

[11] D. V. Skryabin, F. Luan, J. C. Knight & P. S. Russell. "Soliton self-frequency shift cancellation in photonic crystal fibers." *Science* **301,** 1705–1708, (2003).

[12] G. P. Agrawal. *Nonlinear fiber optics* Ch. 10, 12 (Academic Press, Boston, 2007).

[13] Z. W. Bao, M. Miyagi & S. Kawakami. "Measurements of field deformations caused by bends in a single-mode optical fiber." *Appl Opt.* **22,** 3678-3680, (1983)

[14] I. Verrier & J. P. Goure. "Effects of bending on multimode step-index fibers." *Opt. Lett.* **15,** 15-18 (1990).

[15] J. Nicholson *et al.* "Demonstration of bend-induced nonlinearities in large-mode-area fibers." *Opt. Lett.* **32,** 2562-2564 (2007).

[16] J. Cheng *et al.* "Time-domain multimode dispersion measurement in a higher-order-mode fiber." *Opt. Lett.* **37,** 347-349 (2012).

CHAPTER 6

TIME-DOMAIN DISPERSION MEASUREMENT IN HIGHER-ORDER-MODE FIBER

6.1 Introduction

Solid silica-based higher-order-mode (HOM) fibers can copropagate light in different modes without intermodal coupling [1]. Specific modes in HOM fibers, such as the LP_{02} mode, can be designed to have large anomalous dispersion and effective mode area (A_{eff}). The combination of the large anomalous dispersion and the small nonlinearity due to the large A_{eff} is desired for many practical applications, such as dispersion compensation, high energy pulse delivery, and high power amplification [2-4]. This combination also enabled HOM fibers to produce soliton with approximately 1 nanojoule pulse energy at a variety of wavelengths [5, 6]. According to the soliton condition, even higher pulse energy can be achieved by increasing the anomalous dispersion [7]. In addition, HOM fibers or few mode fibers have recently received significant attention as a possible way to improve the performance of fiber transmission and increase the data capacity by mode-division multiplexed transmission [8-10]. As the dispersion value of HOM fibers is of great importance, a method that conveniently and precisely measures the dispersion of HOM fibers can significantly facilitate the fiber design process.

Dispersion measurement techniques for single-mode fibers (SMFs), including time-of-flight technique, phase-shift technique, and interferometric technique, can be used to characterize the dispersion of HOM fibers with only one mode excited. These techniques

cannot be directly applied to measure the dispersion of HOM fibers with multiple excited modes. Various multimode dispersion measurement techniques were developed in the past to characterize multimode fibers (MMF), including HOM fibers [11-14]. The majority of these techniques are based on interferometry, which measure the spectral fringes caused by the intermodal interference in HOM fibers. The interference after a few meters of fibers can be directly measured using an optical spectrum analyzer (OSA) [11]; the interference after several kilometers of fibers can be observed with an electrical spectrum analyzer [12]. Spectral fringes can also be mapped to a time-domain signal by using a light source that sweeps the wavelength at a constant rate, or real-time optical Fourier transformation [13, 14]. The beat frequencies of the interference fringe can be extracted through Fourier transformation, which correspond to modal delays between two different modes within the fiber. The wavelength-dependence of the modal delays indicates the relative dispersion between these two modes. To measure the absolute dispersion of each mode in the HOM fiber, a reference fiber with known dispersion value needs to be added to form a Mach-Zehnder interferometer with the test HOM fiber. Modal interference between light in the HOM fiber and the reference fiber has to be separated out from the intermodal interference within the HOM fiber in order to obtain the absolute dispersion [15]. A free-space interferometer with a CCD camera has also been used to characterize the relative modal delay and mode profile in a short piece of multimode fiber [16]. However, this technique requires cross-correlation to measure the delay at each wavelength, which significantly limits its efficiency for broadband dispersion measurement and its practicality for real-time applications. All these interferometric techniques are sensitive to noises introduced by environmental instabilities, and are relatively complicated to implement. In this paper, we demonstrate a convenient time-domain technique to achieve

simultaneous multimode dispersion measurement in a new HOM fiber, which aims to achieve higher anomalous dispersion at 1064 nm in the LP_{02} mode than previous designs. This technique is based on the standard differential mode delay (DMD) measurement method for MMF [17], and obtains the absolute dispersion of each mode through the wavelength-dependence of its delay using time-of-flight techniques [18-20]. The dispersion values of LP_{01}, LP_{02} and LP_{11} modes are measured using this technique, and results are in good agreement with theoretical calculations.

6.2 Experimental methods

The experimental setup is shown in Fig. 1. An 80-MHz mode-locked Ti:Sapphire laser is used as the input source. The initial input wavelength is continuously tuned between 1010 nm and 1070 nm with a spectral bandwidth in the range of 10-20 nm. The input bandwidth is then reduced to 1 nm by a tunable wavelength selector, which consists of a grating, a collimating lens, a slit, and a mirror. The incident beam is split by a 50/50 fiber coupler. 50% of the optical power is launched into the HOM fiber under test (10.2 m in length), and the other 50% of optical power propagates in the reference arm, which includes 1.7 m of standard SMF. The total input pulse energy is maintained below 1 pJ to avoid fiber nonlinearity. In the test HOM fiber, LP_{01}, LP_{02}, and LP_{11} mode are simultaneously excited after launch. The output from the HOM fiber is measured by a 30 GHz sampling oscilloscope (Agilent 86100A Infiniium DCA sampling oscilloscope). Due to the limited input spectral bandwidth and short fiber length, the durations of the optical pulses are approximately 2 ps or less, which are well below the impulse response time of the detector (~20 ps). In the reference arm, the optical power is split by a 90/10 fiber coupler. The 90% arm is detected by a 20 GHz detector. The electrical pulse

train is then split by a 50/50 RF coupler to trigger the oscilloscope and provide a reference signal. The 10% arm is fed into an optical spectrum analyzer (OSA) to measure the input wavelength. The methodology of this time-of-flight dispersion measurement technique is explained in Fig. 2.

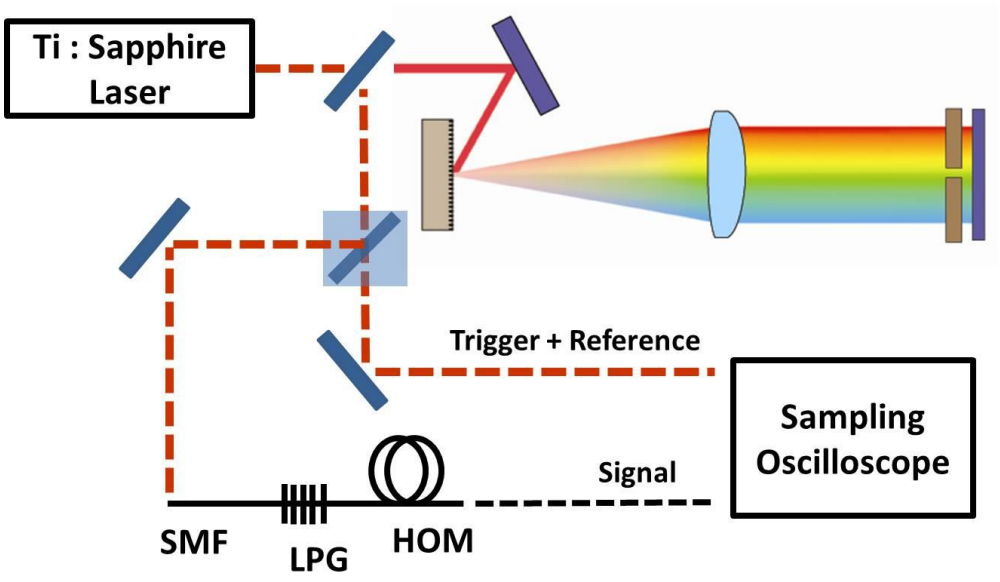

Fig. 1. The experimental setup for measuring the dispersion of an HOM fiber. Free space optical paths and optical fibers are represented by red lines and black lines respectively.

$$D = d\beta_1 / d\lambda = d(T_{delay} / L) / d\lambda \rightarrow d(T_{delay}) / d\lambda$$

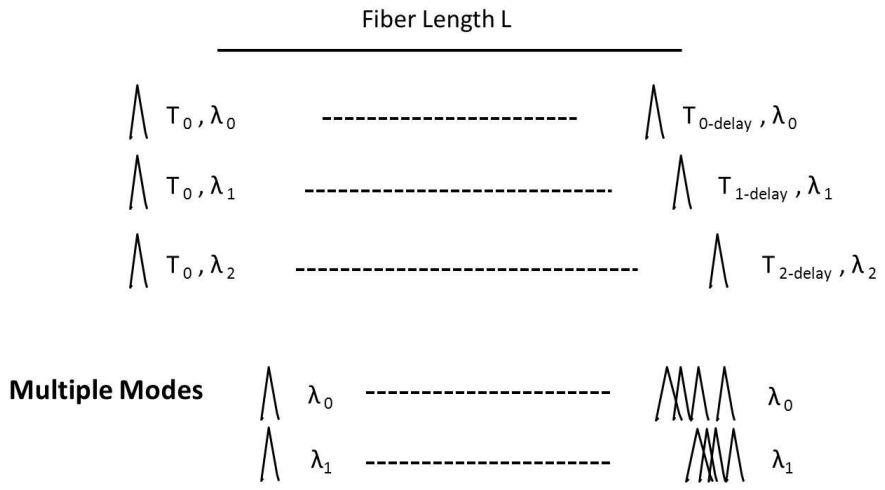

Fig. 2. Schematic drawing of the time-of-flight dispersion measurement technique. Pulses at different wavelengths or modes have temporal delays due to fiber dispersion. The GVD of each mode can be derived by the wavelength dependence of delay for this given mode.

Fig. 3 shows the oscilloscope trace of the HOM fiber output at 1064 nm. The three peaks in the trace correspond to the LP_{01}, LP_{02}, and LP_{11} mode. Each peak is continuously tracked to ensure that it represents the same mode during the wavelength tuning process. The amplitudes of the peaks represent the relative optical power in each excited mode, and the temporal positions of peaks indicate the relative delay of each mode with respect to the reference pulse from the reference arm. At each input wavelength, we measured the relative delay of each mode, which can be expressed as

$$t_0 = t_A - t_R + C = L_A / v_A - L_R / v_R + C \quad (1)$$

where t_0 is the relative delay between mode A and the reference pulse. t_A represents the group delay of mode A through its propagation in the HOM fiber, and t_R represents the group delay of the reference pulse. v_A and v_R are, respectively, the group velocities of mode A in the HOM fiber and the fundamental mode in the standard SMF of the reference arm. L_A and L_R represent, respectively, the length of the HOM fiber and the SMF. C is the constant delay introduced by the RF devices in the system. The measured relative delays of LP_{01}, LP_{02}, and LP_{11} modes as a function of wavelength are shown in Fig. 4. We note that the resolution of the delay measurement is defined by the measured pulse width, which depends on the optical pulse width and the impulse response time of the detector, but the precision of the delay measurement is not limited by the resolution. Delay shift of ~1 ps can be easily measured since the oscilloscope has a temporal precision of 250 fs. In addition, the relative precision of the delay measured can be further improved by using longer lengths of HOM fiber. However, care must be taken to ensure that the relative delay between two modes in the fiber is shorter than the periodicity of the pulse train.

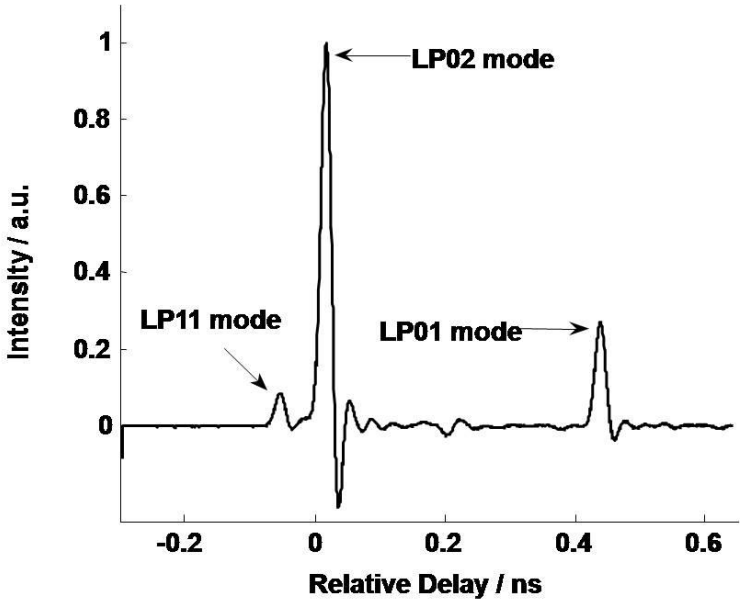

Fig. 3. The oscilloscope trace at 1064 nm input wavelength.

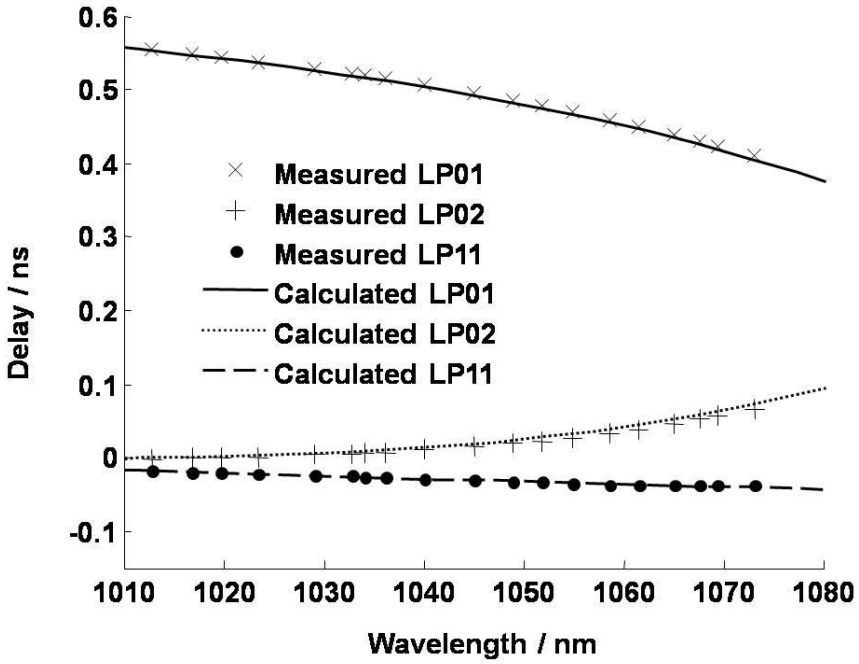

Fig. 4. Measured and calculated delay of LP_{01}, LP_{02}, and LP_{11} mode after 10.2 m of HOM fiber.

The dispersion of one specific mode in the HOM fiber can be calculated from the wavelength-dependence of the relative group delay,

$$D_A = \frac{d(v_A^{-1})}{d\lambda} = \frac{1}{L_A}\frac{dt_A}{d\lambda} = \frac{1}{L_A}\frac{dt_0}{d\lambda} + \frac{L_R}{L_A}D_R \qquad (2)$$

where D_A and D_R are, respectively, the dispersion of mode A in the HOM fiber and the dispersion of the SMF of the reference arm. The relative group delay of each mode (Fig. 3) is fitted to a fourth-order polynomial. The dispersion values are then calculated using Eq. (2) and the polynomial fit. The results are shown in Fig. 4.

We have theoretically calculated the group delay and dispersion for each mode based on the index profile of the HOM fiber. The calculated delay (Fig. 3, unmarked lines) and the calculated dispersion (Fig. 4, unmarked lines) are in good agreement with the measured results. Both the calculation and measurement indicate that large normal and anomalous dispersion were achieved in LP01 and LP02 mode, respectively. The LP02 mode has approximately 200-ps/nm/km anomalous dispersion in the vicinity of 1064 nm, which is valuable for high energy pulse delivery and soliton generation. Small amount of discrepancy exists between the measured and calculated results, as the actual refractive index profile of the HOM fiber may differ slightly from the profile used in the calculation. The discrepancy may also be in part due to the noise in the delay measurement and the deviations of the polynomial fit to the delay data.

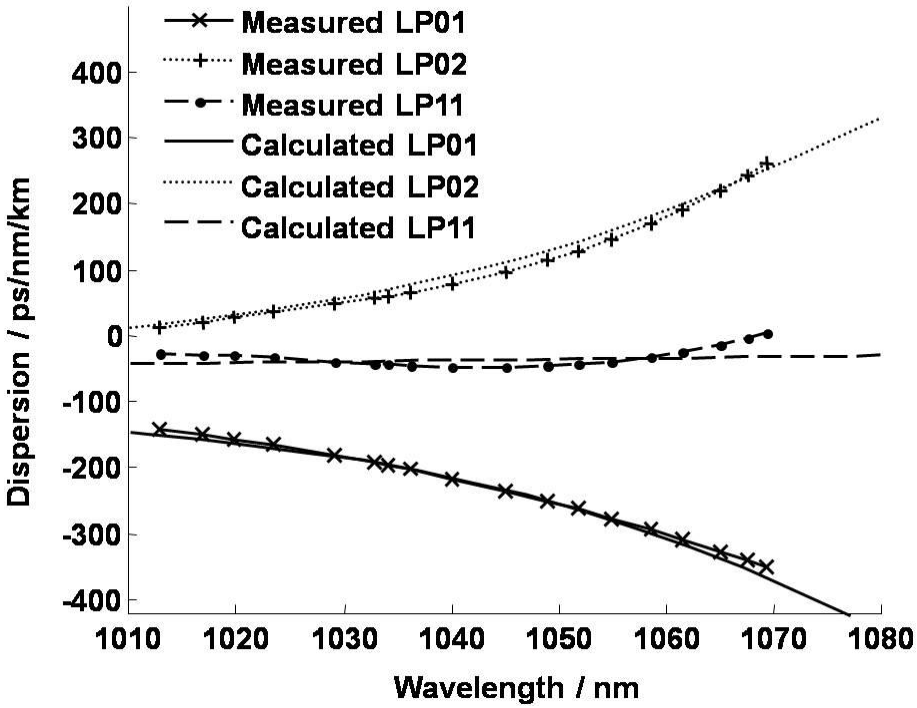

Fig. 4. Measured and calculated dispersion of the LP_{01}, LP_{02}, and LP_{11} mode.

The time-domain dispersion measurement technique presented here has several advantages over the frequency-domain interferometric methods. First, this technique does not require an interferometer, and thus significantly reduces the measurement complexity. Second, this technique directly measures the delay and dispersion in the temporal domain, whereas the delay and dispersion calculated from the frequency-domain information have to be arbitrarily assigned to a specific pair of modes. As a result, this technique eliminates such ambiguities caused by the frequency-domain measurement. Finally, the time-domain technique has the capability of directly monitoring and measuring the power of each mode at different wavelength. While it is used in our experiment, a tunable mode-locked laser is not required for this technique. Simpler multi-wavelength sources based on standard telecommunication equipment already exist. For example, all-fiber sources generated by intensity modulation and time-lens pulse compression can readily provide picosecond and picojoule pulses that are well suited for such measurements [21, 22].

6.3 Conclusion

In conclusion, a convenient and accurate multimode dispersion measurement technique for HOM fiber has been demonstrated. We have implemented our method to characterize the LP_{11}, LP_{02}, and LP_{01} mode in a newly designed HOM fiber. The measured results match our theoretical calculation quantitatively. This technique provides a practical tool for multimode dispersion characterization, which will facilitate future HOM and multimode fiber design, fabrication, and application.

Acknowledgement

The research is supported in part by NIH R01CA133148 and R21RR024415. The authors thank Watt W. Webb for sharing equipment.

REFERENCES

30. S. Ramachandran, S. Ghalmi, J. W. Nicholson, M. F. Yan, P. Wisk, E. Monberg, and F. V. Dimarcello, "Anomalous dispersion in a solid, silica-based fiber," Opt. Lett. 31, 2532-2534 (2006).
31. S. Ramachandran, B. Mikkelsen, L. C. Cowsar, M. F. Yan, G. Raybon, L. Boivin, M. Fishteyn, W. A. Reed, P. Wisk, D. Brownlow, R. G. Huff, and L. Gruner-Nielsen, "All-fiber grating-based higher order mode dispersion compensator for broad-band compensation and 1000-km transmission at 40 Gb/s," IEEE Photon. Tech. Lett. 13, 632–634 (2001).
32. S. Ramachandran, M. F. Yan, J. Jasapara, P. Wisk, S.Ghalmi, E. Monberg, and F. V. Dimarcello, "High-energy (nanojoule) femtosecond pulse delivery with record dispersion higher-order mode fiber," Opt. Lett. 30, 3225–3227 (2005).
33. S. Ramachandran, J. M. Fini, M. Mermelstein, J. W. Nicholson, S. Ghalmi, and M. F. Yan, "Ultra-large effective-area, higher-order mode fibers: a new strategy for high-power lasers," Laser Photonics Rev. 2-6, 429–448 (2008).
34. J. van Howe, J. H. Lee, S. Zhou, F. Wise, C. Xu, S. Ramachandran, S. Ghalmi, and M. F. Yan, "Demonstration of soliton self-frequency shift below 1300 nm in higher-order mode, solid silica-based fiber," Opt. Lett. 32, 340-342 (2007).
35. J. H. Lee, J. van Howe, C. Xu, and X. Liu, "Soliton Self-Frequency Shift: Experimental Demonstrations and Applications," J. Sel. Topics in Quantum Elec. 14-3, 713-723 (2008).
36. G. P. Agrawal, "Optical Solitons" in Nonlinear Fiber Optics, 4th ed. (Academic Press, Boston, 2007), Chapter 5, 132-134.
37. F. Yaman, N. Bai, B. Zhu, T. Wang, and G. Li, "Long distance transmission in few-mode fibers," Opt. Express 18, 13250–13257 (2010).

38. S. Randel, R. Ryf, A. Sierra, P. J. Winzer, A. H..Gnauck, C. A. Bolle, R.J. Essiambre, D. W. Peckham, A. McCurdy, and R. Lingle, "6×56-Gb/s mode-division multiplexed transmission over 33-km few-mode fiber enabled by 6×6 MIMO equalization", Optics Express 19, 16697-16707 (2011)

39. C. Koebele, M. Salsi, D. Sperti, P. Tran, P. Brindel, H. Mardoyan, S. Bigo, A. Boutin, F. Verluise, P. Sillard, M. Astruc, L. Provost, F. Cerou, and G. Charlet, "Two mode transmission at 2x100Gb/s, over 40km-long prototype few-mode fiber, using LCOS-based programmable mode multiplexer and demultiplexer," Opt. Express 19, 16593-16600 (2011).

40. D. Menashe, M. Tur, and Y. Danziger, "Interferometric technique for measuring dispersion of high order modes in optical fibers," Electron. Lett. 37-24, 1439–1440 (2001).

41. J. W. Nicholson, S. Ramachandran, S. Ghalmi, E. Monberg, F. DiMarcello, M. Yan, P. Wisk and J. Fleming, "Electrical spectrum measurements of dispersion in higher order mode fibers" IEEE Photon. Tech. Lett. 15, 831 (2003).

42. T.-J. Ahn, Y. Jung, K. Oh, and D. Y. Kim, "Optical frequency-domain chromatic dispersion measurement method for higher-order-modes in an optical fiber," Opt. Express 13, 10040–10048 (2005).

43. T.-J. Ahn, Y. Park, D.J. Moss, S. Ramachandran, J. Azaña, "Frequency-domain modal delay measurement for higher-order-mode fiber based on stretched pulse interference. " Opt. Lett. 33,19 – 21 (2008).

44. T.-J.Ahn, S. Moon, S. Kim, K. Oh,D.Y.Kim,K. Schuster, and J. Kirchhof, "Frequency-domain intermodal interferometer for the bandwidth measurement of a multimode fiber," Appl. Opt. 45, 8238 – 8243, (2006).

45. Y. Z. Ma, Y. Sych, G. Onishchukov, S. Ramachandran, U. Peschel, B. Schmauss and G. Leuchs, "Fiber-modes and fiber-anisotropy characterization using low-coherence interferometry," Appl. Phys. B. 96, 345-353, (2009).
46. "Differential mode delay measurement of multimode fiber in the time domain," Standard document TIA-455-220-A (Telecommunication Industry Association 2003).
47. B. Luther-Davies, D. N. Payne, and W. A. Gambling, "Evaluation of material dispersion in low-loss phosphosilicate-core optical fibres," Opt. Commun. 13, 84-88 (1975).
48. L. G. Cohen and C. Lin, "Pulse delay measurements in the zero material dispersion wavelength region for optical fibers," Appl. Opt, 16, 3136-3139, (1977).
49. D. Ouzounov, D. Homoelle, W. Zipfel, W. W. Webb, A. L. Gaeta, J. A. West, J. C. Fajardo, and K. W. Koch, "Dispersion measurements of microstructured fibers using femtosecond laser pulses," Opt. Commun. 192, 219–223 (2001).
50. J. Van Howe, J. Hansryd and C. Xu "Novel multi-wavelength pulsed source with time lens compression" Opt. Lett. 29, 1470-1472 (2004).
51. K. Wang and C. Xu, "Wavelength-tunable high-energy soliton pulse generation from a large-mode-area fiber pumped by a time-lens source," Opt. Lett. 36, 942-944, (2011)